Biomedical Signal Processing and Control 93 (2024) 106179

Contents lists available at ScienceDirect

Biomedical Signal Processing and Control

journal homepage: www.elsevier.com/locate/bspc

A review on machine learning in flexible surgical and interventional robots: Where we are and where we are going

Di Wu [a,b,*,1], Renchi Zhang [i,e,1], Ameya Pore [c,g], Diego Dall'Alba [c], Xuan Thao Ha [a,d], Zhen Li [f,b], Yao Zhang [a], Fernando Herrera [a,h], Mouloud Ourak [a], Wojtek Kowalczyk [e], Elena De Momi [f], Alícia Casals [g], Jenny Dankelman [b], Jens Kober [i], Arianna Menciassi [d], Paolo Fiorini [c], Emmanuel Vander Poorten [a]

[a] Department of Mechanical Engineering, KU Leuven, Belgium
[b] Department of Biomechanical Engineering, Delft University of Technology, The Netherlands
[c] Department of Computer Science, University of Verona, Italy
[d] The BioRobotics Institute, Scuola Superiore Sant'Anna of Pisa, Italy
[e] Leiden Institute of Advanced Computer Science (LIACS), Leiden University, The Netherlands
[f] Department of Electronics Information and Bioengineering, Politecnico di Milano, Milan, Italy
[g] Center of Research in Biomedical Engineering, Universitat Politècnica de Catalunya, Barcelona, Spain
[h] ICube, University of Strasbourg, France
[i] Department of Cognitive Robotics, Delft University of Technology, The Netherlands

ARTICLE INFO

Keywords:
Flexible surgical and interventional robots
Machine learning
Modeling
Control
Sensing
Navigation

ABSTRACT

Minimally Invasive Procedures (MIPs) emerged as an alternative to more invasive surgical approaches, offering patient benefits such as smaller incisions, less pain, and shorter hospital stay. In one class of MIPs, where natural body lumens or small incisions are used to access deeper anatomical locations, Flexible Surgical and Interventional Robots (FSIRs) such as catheters and endoscopes are widely used. Due to their flexible and compliant nature, FSIRs can be inserted via natural orifices or small incisions, then moved towards hard-to-reach targets to perform interventional tasks. However, existing FSIRs are confronted with challenges in sensing, control, and navigation. These issues stem from the robot's non-linear behavior and the intricate nature of the lumens, where accurately modeling the complex interactions and disturbances proves to be exceptionally difficult. The rapid advances in Machine Learning (ML) have facilitated the widespread adoption of ML techniques in FSIRs. This article provides an overview of these efforts by first introducing a classification of existing ML algorithms, including traditional ML methods and modern Deep Learning (DL) approaches, commonly used in FSIRs. Next, the use of ML algorithms is surveyed per sub-domain, namely for perception, modeling, control, and navigation. Trends, popularity, strengths, and/or limitations of different ML algorithms are analyzed. The different roles that ML plays among tasks are investigated and described. Finally, discussions are conducted on the limitations and the prospects of ML in MIPs.

1. Introduction

Minimally Invasive Procedures (MIPs) have revolutionized the field of surgery since their advent in the 1980s [1]. Small wounds, shorter recovery time, and improved cosmesis [2], all these benefits favored the adoption of MIPs with respect to more invasive open surgical procedures over the past decades. Currently, MIPs are adopted in different medical specialties, and thence formed different sub-types, such as natural orifice procedure (e.g. colonoscopy, ureteroscopy), endovascular catheterization, and minimally invasive brain surgery [3]. In MIPs, one/multiple small incisions are made, or natural openings are used to access the body and reach target areas of interest. Commonly, MIPs' access port is narrow and the lumen is tortuous, so it is advantageous to use snake-like instruments, such as catheters and flexible endoscopes, since they can reach deeper areas in the lumen. Currently, the (steerable) instruments commonly used in clinical practice are manually controlled. This makes the MIPs highly skill-intensive.

* Corresponding author at: Department of Mechanical Engineering, KU Leuven, Belgium and Department of Biomechanical Engineering, Delft University of Technology, The Netherlands.
E-mail address: di.wu@kuleuven.be (D. Wu).
[1] Equal Contribution.

https://doi.org/10.1016/j.bspc.2024.106179
Received 21 July 2023; Received in revised form 14 December 2023; Accepted 28 February 2024
Available online 15 March 2024

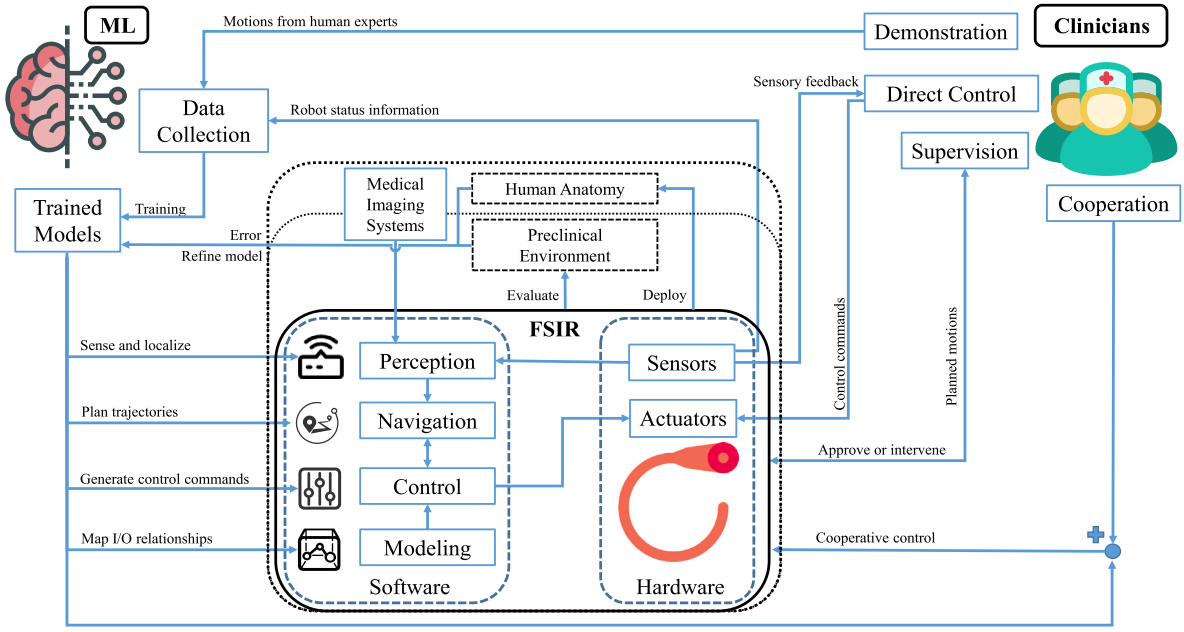

Fig. 1. An overview of the interactions between ML algorithms, clinicians, and FSIRs in robotically-assisted MIPs. The clinicians can control the FSIRs directly with sensory feedback or cooperatively with the assistance of ML. The ML can be trained by the data collected from the FSIRs, or by the demonstration data of expert clinicians. To enhance safety, the clinicians need to supervise the whole workflow when ML is used.

Flexible Surgical and Interventional Robots (FSIRs) have emerged to overcome the limitations of the current (steerable) clinical instruments and to make these approaches less complex for clinicians. FSIRs refer to those snake-like steerable instruments of which one or more of the degrees of freedom (DOF) can be commanded in a computer-controller fashion. FSIRs take advantage of headways in different robotic fields: actuation, sensing, manipulation, and control. Different design and manufacturing approaches have been used to implement FSIRs, thus making the structure or embodiments of FSIRs different. In this paper, FSIRs refer to all snake-like robots used for MIPs: single/multi-backbone "continuum" robots [4], concentric tube robots (CTRs) [5] also known as concentric tube continuum robots (CTCRs) [6], multi-joint flexible robots [7], and flexible needles [8]. FSIRs have demonstrated superiority in accessing hard-to-reach locations in the complex, soft and tortuous internal environment of the human body [9–11]. Moreover, they could offer a higher level of autonomy, intuitiveness, and precision than passive flexible instruments [12]. The use of FSIRs could potentially reduce the mental burden during both challenging and routine tasks, so that clinicians can devote more attention to important aspects or other critical tasks.

1.1. Challenges in current FSIR systems

Current FSIRs share some challenges [12], due to both internal and external factors. Internal factors are determined by the nature of the flexible instrument itself. Most of the recently proposed FSIRs, depending on their structure, are hyper-redundant. A hyper-redundant structure commonly requires a large number of actuators, which further increases the difficulty of controlling the FSIRs. In addition, several factors introduce significant nonlinearities in the FSIRs, such as the intrinsic compliance, viscoelasticity of the manufacturing material, hysteretic behavior in actuation methods, as well as friction between different parts [3]. The nonlinearity of FSIRs means that the system output does not depends only on the current input, but also on previous inputs. This phenomenon makes FSIRs hard to model and control. In clinical scenarios, systematic nonlinearity of FSIRs, if not adequately compensated, would cause imprecise positioning of the FSIRs. This may damage the tissues, and potentially increase the risks in MIPs.

Concerning external factors, the complex anatomical environment creates challenges for the FSIRs. In MIPs, the FSIRs have to go through narrow openings and lumens to reach target positions that locate deeply inside the human body [10,13]. Even more challenging, MIPs, either conventional or robot-assisted, are commonly carried out with a loss of vision and hand-eye coordination, as well as a lack of haptic feedback. During MIPs, avoiding obstacles or hazardous areas (such as the cardiac calcification areas), and reducing the unexpected contact with the lumen walls make the robot path planning and control extremely challenging. Furthermore, anatomical structures vary among different gender, age, or race [14], which raises the demands on FSIRs' adaptability and generality. Control is further complicated by the environment being dynamic, and influenced by the physiological movements, such as heartbeat [15], breathing [16] or blood flow [17]. Another factor that makes control difficult is the compliance and the deformation of the organs, such as bladder or colon. As a consequence, FSIRs needs to be more compliant and also respond more dynamically [18]. Managing all these complex aspects simultaneously is very mentally demanding for a human operator, so the use of FSIRs and the application of assistance techniques that can support the execution of MIPs will play a crucial role in improving these interventional approaches.

1.2. Workflow and tasks of FSIR systems

A typical workflow of robot-assisted surgery could be summarized by a sequence of three phases: sensing, planning, and acting [19]. These phases correspond to three tasks, i.e., perception, navigation, and control. These tasks, together with the modeling, constitute the four primary FSIRs tasks discussed in this work and are visualized in Fig. 1.

The perception capabilities of the FSIR are derived from intra-operative sensors that are integrated directly into the FSIR, or from medical imaging systems such as Fluoroscopy, ultrasound, Computed Tomography (CT), or Magnetic Resonance Imaging (MRI), which are located externally to the patient. Utilizing the data gathered from both the onboard sensors and the external imaging systems, the FSIR can effectively gather critical information about its operational status, the surrounding anatomical environment, and the progression of the current task or the overall procedure.

Table 1
General pros and cons of ML approaches.

Pros	Cons
• No need to understand the underlying physics. No simplifications and assumptions required	• Involving more uncertainty due to the lack of interpretability (cause of a decision)
• Flexible transferability to different tasks with few expert knowledge	• Significant computational resources required
• Increasing the level of autonomy and cognitive capabilities of a system	• Model performance depending crucially on the quality and amount of data, or the quality of manual feature engineering

During the navigation phase, the various information perceived, combined with both the task goal and the current status of the procedure, are used by the planner to plan the robot's motions.

As for the control, the controller computes the commands according to the previously planned motions from the navigation, and sends them to the actuators. Accurate modeling of the robot system make the input/output relations clear, thus is crucial for control accuracy.

1.3. Motivation for machine learning in FSIRs

An increasing number of researchers started investigating ML-based methods to overcome the existing challenges in FSIRs. The objective of ML is to enable a system to gain knowledge by "learning" from examples or experience (training data), and then to make predictions or represent regularities from the acquired knowledge. The learned knowledge could be used in different tasks, such as recognizing the hidden patterns in data, or generating a mapping between input and output, depending on the applications.

In the context of FSIRs, the use of ML methods could avoid complicated modeling and its associated cumbersome parameter identification procedures. ML can capture the underlying patterns from data generated by the system [20]. Additionally, ML-based approaches are observed to have good generalization capability, which allows them to be possibly transferred among different types of robots and different anatomical environments [21–23]. ML could potentially increase the level of autonomy and cognitive capabilities of FSIRs [24]. Consequently, applying ML to FSIRs could potentially free the surgeon or interventionist from routine tasks and allow increased focus on higher-level tasks such as decision-making. ML-assisted FSIRs could also potentially lead to faster execution of routine tasks or lead to higher precision and smoother flow or trajectories compared to manual operation by human experts [24]. In the context of the FSIRs, ML approaches are generally considered to have pros and cons [24–26] as shown in Table 1. The roles of ML algorithms, clinicians and the FSIRs are summarized in Fig. 1. The figure shows that data to train ML algorithms could be collected from clinicians (e.g. human motions) or FSIRs (e.g. actuators' status, shape and pose of the FSIRs). In recent years, the data collected from FSIRs systems has experienced a progressive growth. This has supported the adoption of data-driven approaches such as ML. The trained ML algorithms are utilized for perception, navigation, control, and modeling of the FSIRs. Clinicians may provide demonstrations for training data [27,28], exert direct control over the FSIRs, supervise the FSIRs [29,30], or collaborate with the FSIRs during different phases of the MIPs [31]. The FSIRs can alleviate the burden on clinicians in both mental/cognitive and physical aspects [24].

ML requires distinct training and testing processes. As depicted in Fig. 1, data for training ML models can be gathered while the robot operates in a "preclinical environment". This encompasses various settings, including *in-silico, in-vitro, ex-vivo* environment, and preclinical animal tests. Training may also be continued during or complemented by data collected during real interventions. Once the model is trained, it can then be applied in actual surgical or interventional scenarios. At this point a continuous assessment is expected to quickly identify discrepancies. This approach ensures the model is well-prepared and validated for real-world applications.

Table 2
Abbreviations List of Terminology (in alphabetical order within each ML category)

Category	Terminology	Abbr.
Deep Learning (DL)	Artificial Neural Network	ANN
	Convolutional Neural Network	CNN
	Generative Adversarial Network	GAN
	Long Short-Term Memory	LSTM
	Multilayer Perceptron	MLP
	Recurrent Neural Network	RNN
Reinforcement Learning (RL)	Deep Deterministic Policy Gradient	DDPG
	Deep Q-Networks	DQN
	Deep Reinforcement Learning	DRL
Traditional Machine Learning (ML)	Gaussian Mixture Model	GMM
	Gaussian Mixture Regression	GMR
	Gaussian Process Regression	GPR
	Hidden Markov Model	HMM
	k-Nearest Neighbors	kNN
	k-Nearest Neighbors Regression	kNNR
	Markov Decision Process	MDP
	Random Forest	RF
	Support Vector Machine	SVM
	Extreme Learning Machine	ELM

1.4. Contributions

Over the past years, some review articles have introduced a specific aspects of FSIRs related to fabrication [12], actuation [3,9,12,18], sensing [18], modeling [9,11,12,18], imaging and navigation [10,32], and control [9,11,12,18]. Specific ML techniques are partially discussed in some of these reviews, but do not constitute their main contents. Some other reviews focus on the usage of ML techniques across the entire surgical robotics field [19,24], while their discussion on the FSIRs is sparse. ML used in soft robots has been reviewed in [33], but this work considers generic contexts without a specific link to clinical applications. Moreover, some of these reviews were published more than five years ago [9,10,19,24,32]. Given that ML techniques have gained popularity in recent years, it makes sense to revisit the conducted works to capture the most recent trends.

To the best of the authors' knowledge, no previous review has been carried out for ML techniques specifically used on FSIRs. This survey aims to bridge this gap by providing an overview of ML, including both traditional ML approaches and modern DL approaches, and by discussing how to leverage ML in various FSIRs tasks. It also addresses the limitations and perspectives of ML algorithms within the FSIRs context. The paper is structured as follows: Section 2 introduces ML techniques and a 2D classification method for classifying all ML techniques; Section 3 describes the search method for bibliographies and the inclusion criteria; the ML methods used in various FSIRs tasks, namely perception, modeling, control, and navigation, are summarized, discussed, and compared in Section 4. Section 5 addresses the current challenges in ML, and Section 6 concludes the paper.

2. Introduction to machine learning

ML has emerged as a mainstream aspect of Artificial Intelligence (AI), characterized by its ability to learn or be trained from data. This contrasts with other areas of AI, such as Good Old-Fashioned Artificial Intelligence (GOFAI) [34,35], which predominantly relies on human-defined rules and logic. ML have demonstrated its capability to solve complex real-world problems in different domains without building task-specific models. ML is described as "*programming computers to optimize a performance criterion using example data or past experience*" [36]. Current ML algorithms can be divided into three main

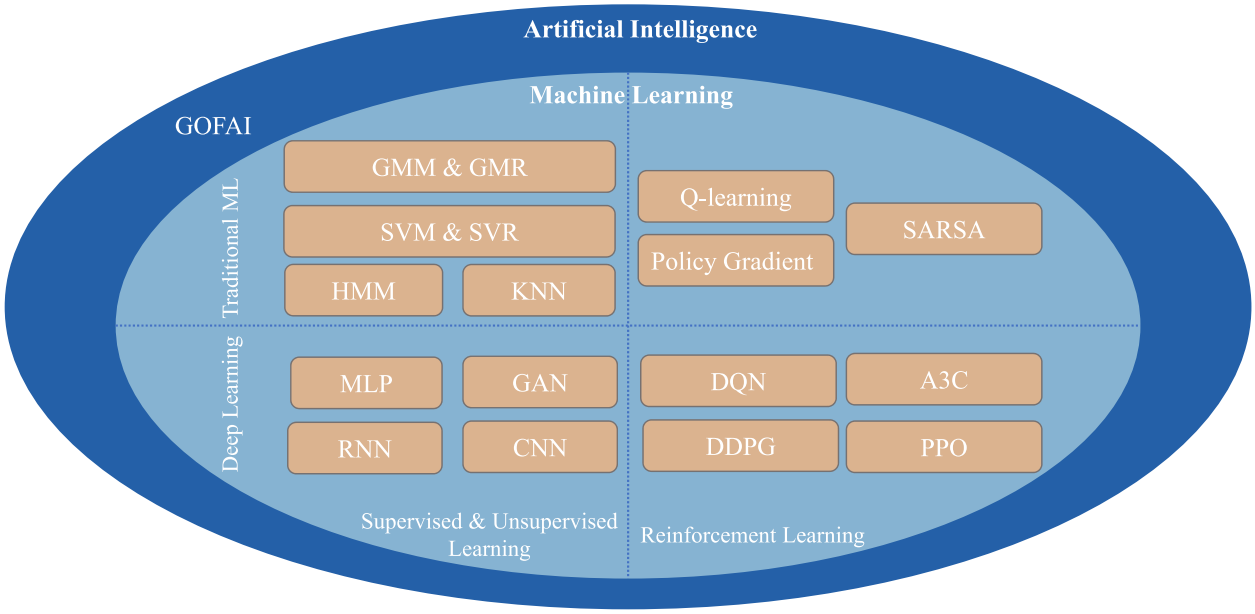

Fig. 2. A Venn diagram of AI techniques applied on FSIRs: ML, comprising traditional ML and DL, is the dominant subdiscipline of AI. One example that belongs to AI but not to ML is "Good Old-Fashioned Artificial Intelligence" (GOFAI), which relies on rules and logic explicitly programmed by humans and does not involve a learning procedure. Several specific ML algorithms often used in the FSIRs are also indicated here. Refer to Table 2 for the abbreviations of the different ML algorithms.

categories: supervised learning, unsupervised learning, and reinforcement learning (RL) [37]. Supervised learning learns the mapping from input data to ground truth (labels) using annotated datasets, while unsupervised learning learns to discover regularities solely from the input data. Rather than learning from input data, RL trains an agent while interacting with the environment using a system of reward and punishment, thus learning from the agent's experience [38]. Although the conventional classification presented is clear and concise, it is not instructive enough to represent all applications of ML algorithms used in different tasks of FSIRs with sufficient detail. Thus, we propose a two-dimensional (2D) classification method (see Fig. 2) for ML, as this representation may provide an additional perspective on algorithm choice for FSIRs applications. The conventional classification mentioned above (supervised learning, unsupervised learning, and RL) is retained as the first dimension in the proposed 2D classification; however, supervised and unsupervised learning are merged into a single category. Additionally, in the second dimension, ML algorithms are divided into two categories: traditional ML and deep learning approaches.

In this review, traditional ML refers to algorithms that do not rely on deep Artificial Neural Networks (ANN). This category includes many algorithms that have been extensively studied over a long period. In the past decade, the use of deep ANN has significantly advanced the state of the art in numerous domains, such as visual object detection, natural language processing, and speech recognition [39]. Recently, DL has also been adopted by the FSIRs community. Nonetheless, traditional ML approaches continue to play vital roles in many FSIRs tasks. Therefore, illustrating the applications of both traditional ML and DL across different tasks is beneficial for algorithm selection. The remainder of this section elaborates on the two dimensions of our classification method.

2.1. Supervised, unsupervised and reinforcement learning

Supervised and unsupervised methods are unified in the classification represented in Fig. 2, even though they constitute two distinct categories of ML approaches. This choice is motivated by the fact that many ML methods applied in FSIRs can address both supervised and unsupervised problems, depending on the curated dataset. Supervised learning requires input data along with its corresponding annotations, which can be discrete (for classification) or continuous (for regression). The objective of supervised learning is to discover the mapping between inputs and labels to accurately predict the correct labels for unseen input data. Applications of supervised learning on FSIRs includes learning the kinematics of FSIRs [40], predicting control commands [41], or the status of FSIRs [42], etc. Unsupervised learning does not need labeled data since it discovers the patterns or correlations in the data. Thus, unsupervised learning approaches can be used, for example, to find feasible trajectories of FSIRs in Learning from Demonstration (LfD) tasks [43], or to estimate the depth and motion configurations from the endoscopic image data [44]. The performance of both supervised and unsupervised approaches is always directly related to the quality of the training dataset. However, creating a set of high-quality data can be complex, time-consuming, and human-dependent, especially when preparing annotations for supervised learning.

The third category of ML approaches, Reinforcement Learning (RL), is ideal for situations where the autonomous system can continuously learn from its interactions with the environment through trial-and-error. RL is designed to learn a policy, i.e., a series of correct actions that achieve the goal in defined situations [38]. The training process unfolds as follows: at a specific time, the agent performs an action that results in a new state of the environment. Following this action, the agent receives a reward that is pre-defined. The objective of training is to maximize the cumulative rewards received by the agent. RL has often been employed in control-related tasks, especially in high-level control tasks, as the robot can be trained continuously to adapt to the environment. Its applications in FSIRs are also frequently observed in tasks such as path planning [45] or generating control commands [46]. Unlike supervised and unsupervised methods, training an agent with RL does not rely on well-labeled datasets, which are often a prerequisite for supervised learning algorithms. Instead, it often utilizes a simulated environment where the robot can interact with the environment numerous times.

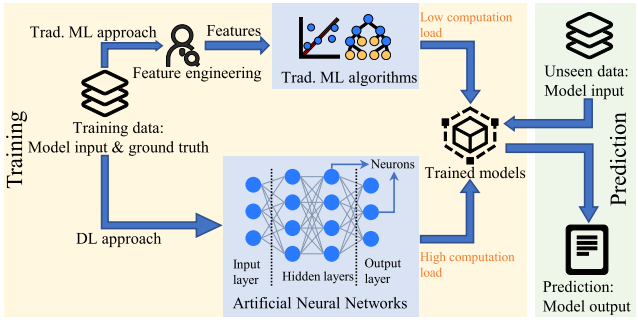

Fig. 3. The comparison between the workflow of traditional ML and DL in supervised learning tasks.

2.2. Traditional ML vs. Deep learning

As introduced in the previous section, traditional ML comprises a group of ML algorithms that are not based on deep ANN. In contrast, DL relies on deep ANN. Optimizing the performance of traditional ML algorithms often involves considerable effort in feature engineering (i.e., transforming raw data into informative and representative values and selecting these values for learning tasks) or applying domain-specific knowledge to preprocess the training data [47] (see Fig. 3). With adequate tuning, traditional ML algorithms can perform relatively well when data is in limited quantities or lower dimensions, such that the preprocessing and feature selection steps are less demanding, or when computational resources are limited [48]. Furthermore, certain traditional ML algorithms, such as linear models and decision trees, are recognized as interpretable models and are easily understood by humans due to their straightforward mathematical and statistical foundations. They can also be utilized to explain the workings of other traditional ML and deep ANN models [49].

The most common traditional ML algorithm employed in FSIRs tasks is the Gaussian Mixture Models (GMM) and Gaussian Mixture Regression (GMR) approach, according to the statistics shown in Fig. 4. GMM is based on the assumption that the input data distribution follows a mixture of multiple Gaussian distributions with their corresponding parameters [37]. Therefore, GMM could represent the joint density of the data. For each Gaussian model, its conditional density and regression function can be derived. GMR utilizes these GMM regression functions to make predictions for new inputs [50]. The GMM-GMR approach is often used in LfD tasks on FSIRs [41,43,51–53]. It can extract the statistical characteristics from noisy demonstration data (i.e., typical when acquiring data from real FSIRs) and predict continuous control commands over time [43]. Based on the statistics in Fig. 4, another popular traditional ML algorithm, the Support Vector Machine (SVM), is also used in FSIRs to tackle classification tasks [54,55].

DL is implemented based on deep ANN. ANN was inspired by the idea of mimicking the working principle of the human brain. However, it is still far from matching the capabilities of human brains at the current stage. A neuron is the basic computational unit of an ANN, connected to several inputs and providing outputs. To generate outputs, a neuron multiplies the inputs by their corresponding weights and then applies a non-linear activation function. Multiple neurons at the same level form a layer. When these layers connect with other layers, an ANN is formed (see ANN in Fig. 3). The input layer of an ANN is responsible for receiving input data, while the output layer delivers the ANN's prediction. The layers located between the input and output layers are known as hidden layers. Backpropagation was proposed and is used to train deep ANN [56].

In recent years, rapid advances in storage, computing power, and advanced software libraries have boosted DL. Hardware advances allowed a significant reduction of ANN training time, shortening this factor by 100 times and more [57]. At the same time, the explosion of big data offers the possibility of training ANN from huge datasets. Moreover, emerging optimization methods (e.g. Adam), activation functions (e.g. ReLU), and regularization methods (e.g. Dropout) are also driving the development of DL. In addition, the emergence of open-source DL libraries (e.g., Tensorflow, Pytorch, Caffe, and Keras) further support the use and dissemination of DL-based approaches. All of these factors make DL accessible to researchers with various backgrounds [58].

DL avoids the need to craft particular features that extract the essence of the underlying data (see Fig. 3). Feature design is typically critical in traditional ML models, especially when dealing with high-dimensional data. Instead, DL tends to recognize such features automatically during the training by adjusting a large number of ANN parameters. However, there is still room for improving the interpretability of DL methods and thus respond to the growing safety concerns when DL are applied in high-risk contexts such as the medical ones [59]. There are different architectures of ANN among DL algorithms, but only a limited set has been applied on FSIRs.

According to the statistics presented in Fig. 4a, the Multi-layer Perceptron (MLP), also known as the Feedforward Neural Network (FNN), is the most widely used ANN in FSIRs. A reason for the popularity of MLP is its strong capability to model nonlinear relations existing in FSIRs such as kinematics/dynamics modeling [40,60,61]. In addition, MLP adopts a simple architecture, which makes it easy to be implemented and trained.

CNNs are also often used with FSIRs. CNN is a type of ANN that contains convolutional layers. Convolutional layers contain filters/kernels used to extract features efficiently from the high-dimensional input data (e.g., images) by a convolution operation. CNN and its variants have demonstrated their strong capability to deal with high-dimensional data. Therefore, they are often used to process visual cues of FSIRs to achieve visual guidance or predict the current status (e.g., tip orientation, distal-end force) using data from multiple sensors [62–64].

RNN is another category of ANN that is often applied on FSIRs. Unlike MLP and CNN, which only consider the current inputs during training, RNN can consider historical inputs to update their "memory" (i.e., hidden states) to influence its current outputs [65]. This structure allows the RNN to capture sequential information, such as time-series data from the inputs. Within the FSIRs field, RNNs can be used to tackle history-dependent phenomena such as hysteresis, or predict the distal-end status of FSIRs based on proximal information [64,66–68].

Besides the different ANN categories, another area of interest for FSIRs researchers when considering DL is Deep Reinforcement Learning (DRL). DRL, as one of the most fast-moving topics of ML in this decade, is an intersection of DL and RL. DRL is often considered to solve real-world decision-making tasks and has proved to achieve human-like intelligence in many games (e.g., Go, Chess, Dota2) [69–71]. ANN plays different roles in different DRL algorithms. For example, in Deep Q-Networks (DQN) [72], ANN is used as a mapping function to find the relation between the input actions along with states, and the reward values. Recent FSIRs researchers employed DRL algorithms such as DQN and Deep Deterministic Policy Gradient (DDPG) [73] for trajectory optimization, motion planning, and control of the FSIRs [30, 46,74–76].

3. Method

This review conducts a large-scale literature search using the Scopus database, the largest abstract and citation database of peer-reviewed literature [77]. Well-known publishers and databases in the field of FSIRs, such as IEEE Xplore, Elsevier, and Springer, are all indexed by Scopus, making it a logical choice for conducting a literature search.

3.1. Automatic retrieval procedure

With the help of the Scopus Search Application Programming Interface (API), queries can be composed to automatically retrieve works

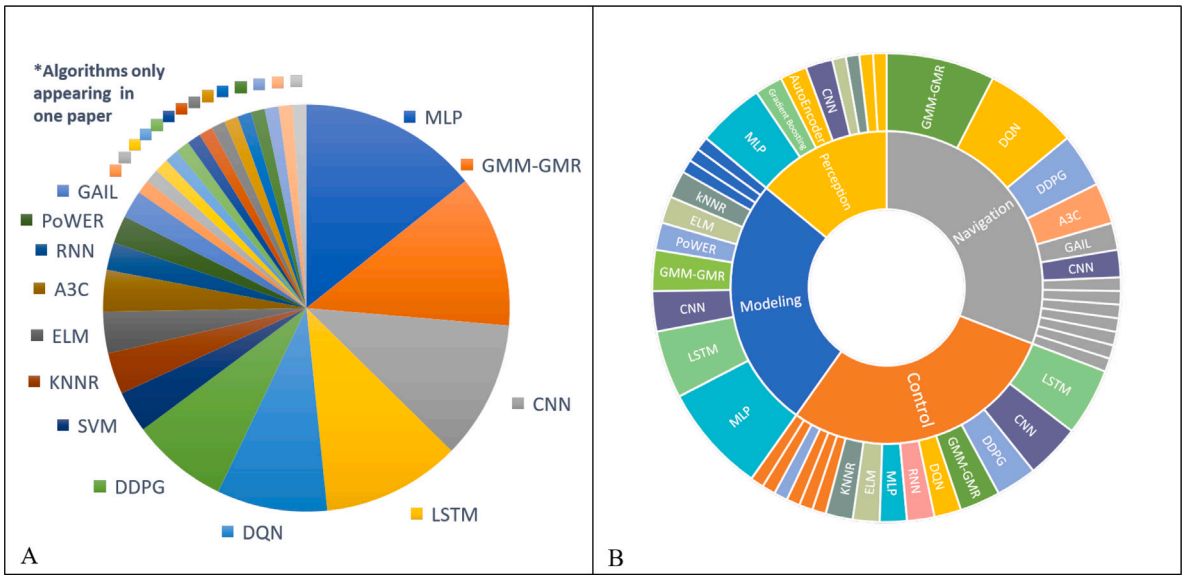

Fig. 4. The popularity of different machine learning algorithms in search results. (A) Proportions of each algorithm in all results. (B) Proportions of each algorithm in different tasks. *Algorithms include UDQL, SARSA, Q-learning, MDP, MA fuzzy Q-learning, LWPR, K-means, HMM, GAIL, BNN, AutoEncoder, Gaussian Process Regression, Gradient Boosting, and ANFIS.

Table 3
Keywords for search. The asterisk wildcard symbol* can include the same combination of letters as the base word.

Algorithm	*AND*	Characteristics	*AND*	System	*AND*	Intervention	OR	Device	
machine learning	*OR*	flex*	*OR*	robot*	*OR*	*vascular*	*OR*	catheter*	*OR*
deep learning	*OR*	continu*	*OR*	automat*	*OR*	percutaneous*	*OR*	*scop*	*OR*
reinforcement learning	*OR*	compliant*	*OR*	assist*	*OR*	cardiac*	*OR*	needle	*OR*
learning-based	*OR*	soft*	*OR*	autonomous	*OR*	colono*	*OR*	dissect*	*OR*
Hidden Markov	*OR*	snake*		guide*	*OR*	uretero*	*OR*	*wire	*OR*
SVM	*OR*					gastro*	*OR*	grasp*	*OR*
Bayesian	*OR*					broncho*	*OR*		
Long Short-Term Memory	*OR*								
Neural Network*	*OR*								
CNN	*OR*								
RNN	*OR*								
LSTM	*OR*								

most relevant to a specific topic. These automated queries were generated using the Python library *pybliometrics*. This library sends requests in the form of a search matrix to the Scopus server [78], which is detailed in Section 3.2. The scope of the query is limited to the title, abstract, and keywords of a paper. This method not only eliminates the need for manual retrieval of relevant works but also prevents duplicate results. Subsequently, results are manually filtered according to the selection criteria, which are outlined in Section 3.3. In addition, both "retrospective" and "prospective" methods were adopted to complete the list of references. The "retrospective" method involves manually screening the bibliography of publications that were retained after manual filtering. In the "prospective" method, papers citing the shortlisted publications are also screened and included if they meet our selection criteria. The final bibliography consists of papers retained after these operations.

3.2. Search matrix

The search matrix was constructed by combining keywords and enriching each keyword with corresponding alternatives. Five keywords were selected to cover the scope of interest for this literature study: ML algorithms, structure of robots, system description, interventional type, and device type. The first keyword ensures that the related works utilize ML algorithms. The second and third keywords limit the retrieved literature to the field of FSIRs. The final two keywords narrow the search to typical medical applications and various types of FSIRs devices.

Two logical operators, *AND* and *OR*, were utilized to guide the Scopus query. The asterisk wildcard symbol was used to broaden the search by retrieving words with the same combination of letters as the base word. This approach allowed for the efficient exploration of the large search space. The employed strategy is believed to cover the vast majority of pertinent literature on this topic. To examine the search space maximally, it is essential to include as many keyword alternatives as possible. However, adding more alternatives can also introduce more unrelated papers. Therefore, a trade-off was made to limit the list of alternative keywords to the most relevant ones. The final search matrix, composed of the final keywords and logical operators, is shown in Table 3.

3.3. Selection criteria

In principle, the retrieved results should closely align with the scope of the review paper. However, even if a paper matches the search matrix well and is related to both ML and FSIRs, it could still be considered out of scope for this review. Papers are deemed eligible only if the authors have directly or indirectly applied ML algorithms in the perception, modeling, control, and navigation of FSIRs. Conversely, papers focused solely on image processing, even if the images are collected by FSIRs, are considered out of scope.

Case 1: Publications on ML-based image processing [79–81] using images obtained by FSIRs are deemed out of scope because they focus purely on image processing. The information from image processing is

Table 4
Applications of ML algorithm in the perception task (yellow for traditional ML, green for DL)

Subtask	Reference	Involved ML Method	Actuation Method	Type of Robot	DoF	Input	Evaluation task	Accuracy
Pose estimation	[82]	LSTM, MLP	Fluidic actuator	CR	2	Resistances of Kirigami Sensors	Estimate posture parameters of the robot	RMSE of posture parameters prediction: 1.27 mm (LSTM), 5.6 mm (MLP)
	[83]	MLP	/	Guidewire	/	Wavelength shifts from FBG sensors	Predict tip position	Predict the shape of a fiber sensor consisting of five FBG triplets with less than 6 mm tip error
	[20]	DL, LSTM	Cable-driven	CR	2	Wavelength shifts from FBG sensors	Estimate 3D shape of the CR	Mean error of 3D shape estimation: 0.66 mm (DNN), 0.69 mm (LSTM); Mean error of distal end position estimation: 0.45 mm (DNN), 0.48 mm (LSTM)
	[84]	DL	Fluidic actuator	CR	2	Wavelength shifts from FBG sensors	Estimate 3D shape of the CR	Mean error of 3D shape estimation: 0.24 mm (3D free-space experiment), 0.49 mm (2D constrained-space experiments)
Contact estimation	[85]	GPR	Fluidic actuator	CR	2	Robot's configuration and actuation	Detect contact state and estimate force direction	Contact state estimation: correctly detects the interactions any time they occur (100% success rate); force direction estimation: the average alignment of estimated and ground truth force direction is 0.95 (where 1 is perfectly aligned, and 0 is orthogonal)
	[86]	Gradient Boosting	Cable-driven	CR	2	Wavelength shifts from FBG sensors	Detect contact state	Contact state estimation: successful detection of collision with hard and soft obstacles within less than 300 milliseconds.
	[87]	AutoEncoder	Cable-driven	CR	2	wavelength shifts from FBG sensors	Estimate contact stage and contact location	Estimate contact stage accuracy: 100% (in at most approximately 1.08 s); Mean contact localization error: 2.3 mm for a 70 mm long CR
	[88]	CNN	Cable-driven	Ablation catheter	2	Optical coherence tomography images	Estimate tip contact and orientation stage	Estimate tip contact stage accuracy: 99.96%; Estimate orientation state accuracy: 92.88%
	[89]	MLP, ELM	Fluidic actuator	Concentric tube CR	2	Actuation input signal and current shape	Estimate tip contact force	RMSE of tip contact force estimation: approximately 65 mN

not applied to the perception, modeling, control, and navigation of the FSIRs.

Case 2: Some works employ ML algorithms for the visual servoing of FSIRs [55,90,91]. Although ML is utilized in image processing in these instances, the outputs of the ML algorithms are ultimately used to control the FSIRs. Therefore, these papers are considered to be within scope.

4. Machine learning applications

As introduced in Section 1.3, ML approaches are widely used across all four tasks/phases considered in this work to address the current challenges of FSIRs (see Fig. 5a) from different perspectives. In the perception phase, ML algorithms can be used to calibrate or model sensors [20], detect collisions and estimate contact forces with the environment [86,89,92], reconstruct the FSIRs's shape [93], or localize the tip [94]. During the navigation phase, ML algorithms generate feasible paths, for example, based on RL [45], learn motion primitives [23], and optimize planned trajectories based on human demonstrations [30,95]. In the control phase, ML algorithms can predict control commands based on the learned Inverse Kinematics (IK) model [52,96], refine parameters of IK-based controllers or PID controllers [43,97], and derive control signals through trial-and-error [46,98]. Refining the information from both Figs. 4b and 5a, it becomes evident that Control is consistently the task where ML is most frequently applied, whether analyzing the total body of literature over the past decade or annually. In modeling, ML algorithms are utilized for modeling the nonlinearities within the continuum FSIRs [60,66,99,100], modeling the kinematics/dynamics [41,101,102], and predicting the distal end status based on proximal information [64,67]. In some cases, ML algorithms are also applied across phases to achieve overall control of the robotic system [43]. An overview of the frequency of occurrence of each ML algorithm in different tasks is provided in Fig. 4.

Regardless of the task considered, since all ML methods are data-driven approaches, their performance is strongly influenced by the training data. Therefore, it is essential to pay careful attention to data collection, which can vary in approach depending on the complexity of the tasks. In lower-level tasks such as modeling and control, the data is usually collected directly from proprioceptive sensors that are embedded in the FSIRs [41,52,63] or placed in the environment [99,103]. For more complex tasks such as navigation, the fusion of proprioceptive and exteroceptive information [55,104] plays an essential role to estimate the state of FSIRs while considering the interaction between FSIRs and the environment. In addition, demonstration data from human expert, animals [105] or even a rigid-link robot [22,106] can be utilized when teaching the FSIRs to complete high-level tasks.

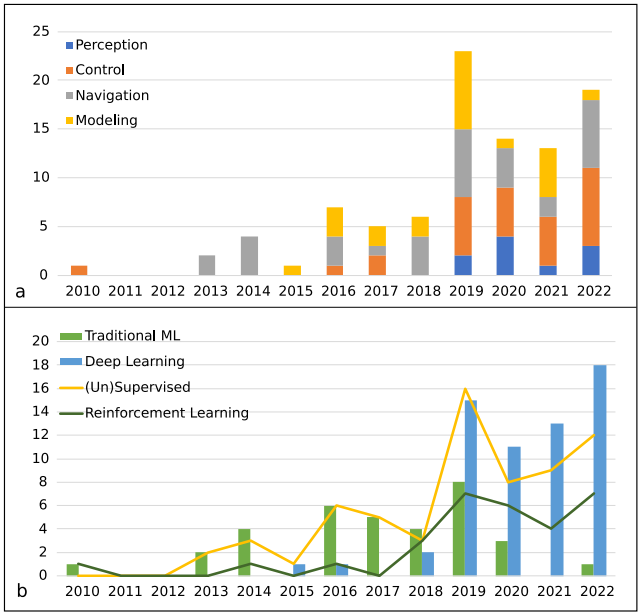

Fig. 5. Evolution of frequency of ML, from 2010 until 2022, used in various FSIRs tasks over the years: (a) the number of publications of each task; (b) count of publications in terms of the proposed 2D classification: Traditional ML versus DL and supervised&unsupervised learning versus RL.

4.1. Perception

If the configuration e.g., pose, shape, and contact state of the FSIRs could be measured, this information could be used to facilitate navigation, and control the FSIRs in an accurate and more gentle fashion. Several methods have been proposed in the literature to improve the awareness of the FSIRs during the procedure. According to Table 4, DL methods (MLP, CNN, and Encoder–decoder) are quite popular in the perception task. Nevertheless, some traditional ML algorithms such as

Gradient boosting and GPR have also been employed in recent years. In this section, different ML-based pose/contact estimation methods are discussed.

4.1.1. Pose estimation

Traditionally, many intraluminal interventions are conducted with the assistance of fluoroscopy, but the ionizing radiation generated by fluoroscopy is harmful for both patients and clinicians. Another limitation of fluoroscopy is that it provides only 2D visualization, requiring clinicians to mentally correlate the obtained 2D information of the FSIRs with the patient's 3D anatomy. Due to these disadvantages, various sensor modalities have been investigated as alternatives to the traditional fluoroscopic system. Several ML-based approaches that utilize information provided by sensors have been developed to track the pose of the FSIRs in real-time, including position tracking and shape sensing, during the MIPs.

Distributed sensors are commonly used to sense the shape of the FSIRs since they do not have the problem of line-of-sight (i.e., it could work inside the patient body). A framework for 3D shape reconstruction of a three-segment soft robot using DL with feedback from proprioceptive sensor skin is described in [82]. The sensor skin was made out of conductive silicone using kirigami. A novel kinematic description linking the entire soft robot's structure to low-dimensional configuration parameters was also proposed. This work demonstrates that an LSTM network can learn the relationship between the sensor's resistance and the configuration parameters.

Fiber Bragg Grating (FBG) is increasingly being used in shape sensing of FSIRs thanks to its tiny size, bio-compatibility, and safety (e.g., being free of the risk of electrocution). The traditional FBG-based shape sensing method starts with calculating the curvature from the measured wavelength shift of FBG sensors distributed along the fiber length. The calculated curvature is then integrated to reconstruct the 3D shape of the fiber. One of the major problems in traditional FBG-based shape sensing methods comes from the inaccuracy in estimating the curvature from the measured wavelength shifts of FBG sensors. Several characteristic parameters of the fiber, *e.g.* strain sensitive coefficient, angles between cores and distance between the central and outer cores, are required to calculate the curvature. However, these parameters vary due to the assembly process, which requires a complex identification process. To overcome this problem, Manavi et al. proposed to train an ANN to extract the shape information directly from the Edge-FBG spectrum [83]. The developed ANN can reconstruct the shape of a fiber sensor made up of five Edge-FBG triplets with an error of less than 6 mm at the tip. To further avoid the consequence of integrating the inaccurate curvatures estimated by traditional FBG-based shape sensing method, Sefati et al. [20] proposed an ANN-based method to directly estimate the tip pose of a continuum manipulator from the measured wavelength shifts of FBG sensors. The continuum manipulator is modeled as a pseudo-rigid body. Then a constrained optimization problem is formulated to solve the joint angles of the continuum manipulator in order to reconstruct the shape. The proposed ANN-based shape sensing method has improved the shape sensing accuracy by approximately 58% compared to the traditional FBG based shape sensing method. However, the method proposed in [20] employs a computationally intensive optimization process which makes it difficult to extend to multi-DOF continuum robot. Ha et al. presented an ANN model that can directly estimate the curvatures at discrete point along the length of the continuum robot providing the wavelength shifts measured by the FBG sensors in [84]. The experimental results show that the presented method in [84] outperforms the traditional FBG-based shape sensing method that relies on the assumption of fiber core's geometry.

Magnetic field based tip pose estimation methods have also received much interest in clinical applications because it is cost-effective and does not require direct line-of-sight. A permanent magnet-based localization for growing robots was presented in [94]. The growing robot is a type of continuum robot that achieves locomotion by extending from their tip. The tracking system includes a permanent magnet integrated into the robot tip, and an array of magneto-inductive sensors that are placed underneath the robot to measure the change in the magnetic field as the robot moves through its workspace. A hybrid strategy that combines dipole model-based localization with trained ANN was proposed in this work. This strategy compensates for the measured flux density of each sensor in order to improve the tip pose estimation accuracy. The presented hybrid approach achieves a position error of 4.3 ± 2.3 mm in a 5-degree of freedom (DOF) setting. The hybrid model improves the position tracking accuracy by approximately 37% (compared to the model-based localization method) when the magnet moves at high speed (*i.e.* 255 mm/s).

4.1.2. Contact estimation

During MIPs, knowledge about the interaction force between FSIRs and the surrounding environment is desirable, in addition to FSIRs's posture. Information on the current contact forces helps improve the awareness of the clinicians or the autonomous system, which allows them to make better decisions during navigation. Embedding force sensors on FSIRs to measure either tip force, distributed force, or contact state is arduous considering the size limitations and the constraints related to cleaning and sterilization. A model-based component was presented as an alternative to direct sensing in [85]. The nonlinear disturbance observer, with corrections learned from data via the ML method namely Gaussian Process Regressors, can estimate the contact state and force direction. The method in [85] requires only the knowledge of the robot's posture and actuation signals. To measure its efficiency, the normalized scalar product of the estimated force direction with the ground truth was evaluated. The average alignment yielded the result of approximately 0.92 (where 1 is perfectly aligned) with a standard deviation of 0.08. Another approach to estimate the contact state of a continuum manipulator was proposed in [86]. This work proposed a trained ANN to directly detect collision from the measured wavelength shifts of the integrated FBG sensors. Experimental results demonstrated successful detection of collision with hard and soft obstacles in less than 300 milliseconds. A data-driven approach to estimate not only the contact state but also the contact location is proposed in [87]. The proposed method requires only the measurement of the curvatures along the length of the robot. In this work, the curvatures are measured by a multi-core optical fiber embedded in the central channel. Experimental results show a mean average localization error of 2.3 mm for a 70 mm long flexible robot.

Knowledge of the interaction force is useful not only for safe navigation but also important for tasks that require maintaining contact between the FSIRs and tissue over a period of time, such as catheter ablation treatment. Yu et al. proposed a method to estimate the contact and orientation based on direct endomyocardial imaging acquired by optical coherence tomography [88]. A CNN-based two-stage classifier was developed to provide an intraprocedural assessment of contact parameters, achieving the accuracies of 99.96% and 92.88% for contact and orientation estimation, respectively. Unlike [85,86,88] which mainly concentrate on estimating the contact state, [89] developed a virtual sensor for estimating the tip contact force of concentric tube continuum robots through supervised learning. This work also shows the usefulness of the transfer learning approach based on deep direct cascade learning. The deep direct cascade network was pre-trained with synthetic data generated by a simulated model of the robot before training with real data. The accuracy of 8.471 ± 1.389 mN in tip contact force estimation was reported in [89]. In [107], a comparative analysis was conducted between four learning-based techniques and a formerly validated mechanistic approach for estimating tip force of a catheter. The results revealed that, upon optimizing the hyperparameters, the accuracy and precision of the learning-based methods outperformed that of the mechanistic model.

Table 5
Applications of ML algorithms in the modeling task (yellow for traditional ML, green for DL and purple for RL)

Subtask	Reference	Involved ML Method	Actuation Method	Type of Robot	DoF	Modeled Object	Evaluation task	Performance
Model Kinematics/Dynamics	[61]	MLP	Simulation	Continuum Robot (CR)	3	IK	Trajector following	RMSE: ca. 0.18 m and ca. 0.21 m (with last 3 joints fixed)
	[108]	MLP	Simulation	Concentric Tube	5	FK, IK	Predicting the tip position, tube extension and orientation	Mean tip error: 0.2 mm, 0.002 difference (FK); Error in tube extension: 0.8 mm, errors in tube rotation 0.1° (IK)
	[40]	MLP	Cable-driven	Concentric Tube	6	FK, IK	Predicting the tip position, tube translation and orientation	RMSE: 2.3 mm in position, 1.1° in orientation (forward) 4.0 mm in position, 8.3° in orientation (inverse)
	[109]	MLP	Cable-driven	Multi-joint	7	FK, IK	Predicting the trajectory	RMSE: 3.047e−07 (forward) mean absolute error: 1.8e−03 (inverse)
	[102]	LSTM	Cable-driven	Multi-joint	7	IK	2D trajectories following	Mean tracking error norm: 3.47 mm (Square)
	[101]	BNN	Cable-driven	Multi-joint	7	Kinematics, Dynamics	Predict tip position and motor torques	Test RMSE: [0.109, 0.145, 0.108]mm (kinematics); [0.037, 0.050, 0.050, 0.024, 0.025]Nm (dynamics)
	[53] [41]	GMM, KNNR	Cable-driven	Serpentine manipulator	2	IK	2D trajectories following	RMSE: 2.5556 mm (GMR), 2.1527 mm (KNNR)
	[96]	LWPR	Fluid-driven	CR	2	IK	3D trajectory following	Mean accuracy: ±2.21° and maximum ±7.49° ; ±2.49° and maximum ±11.03°) with external disturbance
	[52]	GMM	Cable-driven	CR	3	FK, IK	3D trajectory following	RMSE and standard deviation: 1.379±0.637 mm (forward), RMSE 1.909±1.067 mm (inverse)
Model Nonlinearities and Hysteresis	[60]	MLP	Cable-driven	CR	2	Hysteresis	Hysteresis modeling	Error distribution of 0.11 with 81.8% variability in hysteresis
	[66]	LSTM	Fluid-driven	CR	1	Hysteresis	Predict the bending angle with hysteresis	RMSE: 0.36° ; MAE: 1.23° ; NRMSE: 1.17%
	[100]	LSTM, ELM	Cable-driven	CR	2	Backlash	3D trajector following	RMSE: [9.6, 9.1, 9.34]° (LSTM); [12.9, 12.6, 12.0]° (ELM)
	[110]	CNN	Cable-driven	Multi-joint	2	Hysteresis	Pose estimation with hysteresis	Average hysteresis reduction rate of RMSE: 60.24±0.37% at θ_1 and 65.15 ± 0.65% at θ_2
	[111]	MLP	Cable-driven	Multi-joint	2	Hysteresis	Estimate the joint angle of the robot	Maximum hysteresis sizes for 4 degrees: [4.39±1.0, 7.3±0.9, 8.19±0.9, 12.4±1.5]°
	[99]	ELM	Cable-driven	CR	3	IK Hysteresis	2D and 3D trajectories following	RMSE: 0.55 mm (2D), 2.03 mm (3D)
	[112]	ANFIS	Cable-driven	Adapted commercialized catheter	2	Backlash	Path following	Mean displacement: 1.997 mm±0.849 mm; Mean instantaneous velocity: 3.669×10^{-4} mm/sec±10.767 mm/sec
	[113]	PoWER	Cable-driven	CR	3	IK, nonlinearity	2D trajectories following	RMSE after RL refinement: 1.101 mm
	[43]	PoWER, Linear Regression	Cable-driven	Serpentine Manipulator	3	IK, nonlinearity	Tube insertion and circle following	Returns of rollout: 0.986 (tube insertion) and 0.981 (circle following)
Model Distal-end force Feedback	[103]	CNN	/	Guidewire	2	Force mode	Obstacle avoiding	Maximum operating forces: 0.24 to 0.79 N
	[67]	LSTM, MLP	Cable-driven	CR	2	Force	Predict force hysteresis	Average RMSE: 0.1364 N
	[64]	CNN, LSTM	Cable-driven	CR	2	Force	Predict force hysteresis	Average RMSE: 0.1711 N

4.2. Modeling

Researchers have derived different analytical models that are capable of describing the robot kinematics or dynamics to control conventional rigid-link robots. However, in the context of FSIRs, these models tend to be more complex and less precise due to the inherent nonlinear characteristics of FSIRs. Moreover, the increased number of DoFs of FSIRs further complicates the development of these analytical models.

The modeling tasks discussed in this subsection pertain to problems associated with modeling the properties of FSIRs. These properties may include kinematics, dynamics, or shape/pose, as summarized in Table 5. Developing effective and accurate models of these properties can enhance our understanding and description of FSIRs, thereby improving control precision and adaptability to various environments.

According to Fig. 4b, MLP is the most widely used algorithm that accounts for approximately one-third of all the ML algorithms used in the modeling task. This is due to its strong capability to model nonlinearities and its ease of implementation. Other DL algorithms such as LSTM and CNN are also frequently used.

4.2.1. Model kinematics/dynamics

ML algorithms are applied to model the kinematics of FSIRs to avoid the need for analyzing robots' physical properties and complex formulations. These algorithms can be easily transferred among different types of FSIRs, making this a versatile modeling approach. Furthermore, the ML approach, as a data-driven method, collects training data from actual robots. This process helps in identifying patterns within the robotic system, including nonlinear phenomena. This method proves to be especially beneficial for continuum robots, where nonlinearities are significant, compared to traditional kinematics/dynamics models. It is important to note that in this subsection, the included articles focus on modeling the robot kinematics or dynamics for those FSIRs where nonlinearities are not a primary concern, such as multi-joint surgical robots [102], CTRs [40], or instances where compensating for nonlinearities is not highlighted as a key contribution by the authors.

Traditional ML approaches, such as regression and joint probability density models, have been explored to address the modeling problem of FSIRs. A study presented in [53] compares GMR and k-NN regression to learn the IK of a Tendon-Sheath-Mechanism (TSM) robot. The training data is derived from motor movements and end-effector states, obtained through human demonstration, paired together. The study reports average prediction accuracies of 91.2% for GMR and 93.2% for k-NN, considering both actuators in the TSM robot. Further research by [41] introduced the ELM for comparison. The Root Mean Square (RMS) errors of GMR, k-NN Regression, and ELM in trajectory following experiments were 2.5556 mm, 2.1527 mm, and 2.3277 mm, respectively.

Another study, presented in [96], explores a regression method to directly estimate the IK of a redundantly actuated fluidics-driven soft robot. This method trains a global IK model, learned as a weighted sum of several local inverse models, using Locally Weighted Projection Regression in real-time. The initial system, based solely on simulated data, achieved a mean tracking error of ±1.79°. This performance improved to ±0.90° through online learning. Furthermore, Dynamic Gaussian Mixture Model [114], a variant of the GMM, was used in [52] to model both the forward kinematics (FK) and IK of a catheter. This model processes data on the catheter's current and next states alongside the corresponding control actions.

ANN also demonstrates its efficiency to model the kinematics of the FSIRs. When the FSIRs have higher number of DoFs, DL is especially

preferred over traditional ML. This trend is observable in Table 5. In non-clinical applications, non-redundant continuum robots have been shown to benefit from the use of ANN for modeling kinematics, demonstrating superior performance compared to conventional methods as highlighted in previous works [115]. MLP is the most commonly used model in FSIRs tasks, as evidenced by its popularity across reviewed articles, as shown in Fig. 4a. A study for CTR is presented in [108], where MLP was used to learn FK and IK, although it was only tested in simulations. Another study [40,116] applied MLP to learn FK and IK for a 6-DoF concentric tube continuum robot, with data collected from a real-world robotic platform, unlike [108]. The research in [40,116] stands out for publishing a comprehensive dataset comprising 100,000 joint configurations, each paired with a CTR tip pose, recorded using an electromagnetic tracking system.

In [61], the IK learning problem for continuum robots was addressed by carefully selecting and adjusting the training data representation. Here, MLP was chosen as the learning method, with data generated from a simulated kinematic model. The introduction of a new trigonometric joint description enhanced feature representation for model learning. This improved the prediction accuracy, with the FK model achieving less than 2.3 mm in position error and 1.1° in orientation error. For IK, errors were limited to 4.0 mm for translation actuators and 8.3° for rotation actuators. Li et al. explored three different ANN architectures with varying loss functions to model the kinematics of the Micro-IGES, a multi-joint tendon-driven flexible surgical robot [109]. An extension of this work employed LSTM to model the Micro-IGES robot's kinematics [102], demonstrating superior control accuracy compared to traditional Denavit–Hartenberg models. Furthermore, a Bayesian Neural Network (BNN) was used to learn the kinematics and dynamics of the Micro-IGES robot, offering insights into the epistemic uncertainties of the learned system [101]. BNN showed better resistance to overfitting compared to MLP and outperformed a pseudo-inverse kinematic controller in tip positioning accuracy. However, a direct comparison between BNN, MLP, and LSTM is necessary to fully assess BNN's modeling capabilities.

4.2.2. Model nonlinearities and hysteresis

Nonlinearities such as hysteresis, deadzone, and backlash pose significant challenges in FSIRs, drawing considerable attention from researchers. Many articles in this section also essentially model the FK or IK of the FSIRs. However, the nonlinear characteristics of FSIRs discussed here are more pronounced and thus recognized as a major obstacle by researchers, unlike the discussions in the previous section. The systematic nonlinearities in FSIRs stem from factors like their inherent soft structure, internal friction, and interactions within segments. These nonlinearities lead to discrepancies between the anticipated movements of the end effector, based on the actuator motions planned at the proximal end, and the actual movements executed by the distal part. This discrepancy challenges the effective control of FSIRs during MIPs. To understand and model these nonlinear relationships, researchers often collect training data from the robot's movements, which showcase the nonlinear behavior of the system.

Porto et al. introduced an offline learning strategy using ELM to model hysteresis [99]. This approach involves fitting separate ELMs for the inverse rotation model (angle-motor), inverse radius model (radius-motor), inverse y-coordinate translation model (Y-coordinate-motor), and direct bending model (delta-Y-motor), which are then collectively used to determine joint positions. The method was tested through trajectory following experiments, achieving an RMS error of 2.03 mm for 3D trajectories. Instead of isolating the causes of nonlinearity, the authors in [60] suggested modeling the nonlinear relationship with a single MLP, incorporating variables such as displacement and velocity of the proximal part and reusing the last output as an input, essentially employing a naive RNN approach. However, this method only considers the most recent state, which may not fully capture hysteresis's time-dependent nature, where RNNs could offer more effective sequential data handling. Wu et al. utilized an LSTM network to model the rate-dependent hysteresis in a fluidics-driven robotic catheter [66], with training data consisting of air pressure (input) and tip bending angle (output). The LSTM's performance was superior to both a state-of-the-art analytical model, the Deadband Rate-Dependent Prandtl–Ishlinskii (DRDPI), and the conventional ML method, SVR, in trajectory following experiments, showing a 60.1% and 36.0% improvement, respectively, on an arbitrarily varying trajectory. This approach was further developed in [117] to model hysteresis in 1-DoF bi-directional bending using LSTM. Yet, these studies focused on modeling hysteresis rather than its compensation, addressed in later work [118], which proposed an open-loop controller based on LSTM for controlling and compensating hysteresis in a catheter system. This control-LSTM, used as a feedforward free-space catheter controller, demonstrated precision and robustness against severe hysteresis without requiring a separate inversion step for controller application, unlike many traditional analytical hysteresis models such as [119]. Similarly, Jiang et al. modeled the backlash in a two-DoF steerable endoscope using LSTM, which takes bending angles as input to predict the endoscope's 4-way backlash [100]. To handle nonlinear and delayed responses typical in soft robots, Chen et al. employs an offline-trained LSTM network controller to manage the nonlinear and delayed responses exhibited by soft robots. Additionally, an online optimizing kinematics controller is implemented to reduce the errors introduced by the aforementioned LSTM controller [120]. This method enhances the interchangeability of the soft and continuum robots.

Omisore et al. first identified the most significant factors affecting the backlash gap and then developed a closed-loop control system capable of automatically compensating for backlash [112]. This compensation is realized through an Adaptive Neuro Fuzzy Inference System (ANFIS) [121] to predict potential backlash and a force modulation model to monitor contact forces between the catheter tip and vessel walls. In their in-vitro experiment, the mean absolute deviations of the input signal, displacement, and instantaneous velocities were 0.849 mm and 10.767 mm/sec, respectively.

Visual feedback has also been utilized to compensate for the hysteresis. A hysteresis compensator that incorporates learning-based pose estimation was proposed in [110], employing a siamese CNN for tip pose estimation. This method adjusts the position command with additional movement to reduce hysteresis, mimicking the intuitive adjustments made by clinicians using visual feedback. The approach successfully reduced hysteresis by up to 71.4%. Further improvements were achieved by combining this visual-based method with a kinematic-based joint angle estimation technique, reducing hysteresis to less than 5° for sheath configurations of 0° or 90° [111].

Another approach, blending an analytical model with RL, was introduced to address the nonlinearity issue in [43,113]. This method applies RL to compensate for internal system nonlinearities in a 2-DoF TSM. Chen et al. features a three-layer approach: motion planning, IK solver, and RL refinement [43]. Initially, human demonstrations of teleoperating the TSM are recorded and modeled using GMMs. The TSM then executes commands generated from GMR, derived from GMMs as explained in Section 2.2, with end-effector positions recorded to learn the IK model using linear regression. Notably, the GMM-GMR approach is highlighted as one of the most popular traditional ML method reviewed in the related literature according to Fig. 4a. The final layer employs a RL algorithm, Policy Learning by Weighting Exploration with the Returns (PoWER), to refine the IK model based on trajectory tracking by the TSM, though this refined model was initially validated only in simulations through a circle drawing experiment. This work was extended in [113] with real-world evaluations, controlling a serpentine manipulator to follow various trajectories using the refined IK model. The RMS errors of the IK model before and after RL refinement were 9.639 mm and 1.101 mm, respectively.

4.2.3. Model distal-end force feedback

Recognizing the forces exerted on the distal end of FSIRs is crucial for accurately estimating the current robot state and ensuring the safety of MIPs procedures [103]. Despite the importance, accurately capturing force feedback at the distal end is challenging due to sensor placement limitations and the inherent nonlinearities and hysteresis of FSIRs. These challenges have led researchers to investigate sensorless methods for estimating distal-tip forces, which could be leveraged to provide haptic feedback.

Li et al. explored deep learning techniques to predict the distal force of TSMs using measurements from the proximal end. They compared LSTM and MLP against traditional model-based methods in tasks involving tissue manipulation [67]. Additionally, they developed a two-stage data-driven approach utilizing ANN to predict the dynamic distal-end force of a flexible robot [64]. In the first stage, data from probing signals and proximal-end force responses are transformed into 2D images. A CNN classifies these images to estimate the sheath bending angle. In the second stage, the two most accurate LSTM models, chosen based on the classification results, make dynamic predictions of the robot's distal-end force.

4.3. Control

Control is a crucial aspect of robotics, and the flexible nature of FSIRs introduces additional complexity due to their higher DOFs and reduced rigidity, challenging both understanding and controlling these systems. Developing a control scheme that ensures high accuracy and dynamic adaptability of FSIRs in various environments is critical for ensuring surgical safety. This section outlines three control approaches: feedforward control using models, feedback control, and RL-based control, as detailed in Table 6. The feedforward control with models eliminates sensors mounted on the tip of the FSIRs, which is considered challenging due to the size limitation and sterilization constraints. The feedforward control can work in some free-space scenarios, such as inside the heart. However, since open-loop control cannot account for environmental interactions, it is only effective in limited environments. On the other hand, feedback control relies on sensors based on various physical principles (e.g., visual, electromagnetic, or optical). RL is also used to train controllers, which translates the high-level commands to motor skills through robot's interactions with its environment.

According to Fig. 4b, LSTM is identified as the most utilized algorithm in control tasks. Despite its popularity, LSTM does not overwhelmingly dominate this area. The cumulative occurrences of the top four algorithms (LSTM, CNN, DDPG, and GMM-GMR) represent nearly half of all instances in control tasks. The control task exhibits the widest diversity of algorithms compared to other tasks, indicating the absence of a single mainstream algorithm in this domain.

4.3.1. Feed-forward control using models in Section 4.2

In the Modeling section, it is highlighted that ML algorithms are pivotal in learning the IK model of a FSIRs. The acquired IK model takes a desired tip trajectory as input and forecasts control commands for the actuators. With this learned IK model, implementing a feed-forward controller requires minimal effort.

Several articles reviewed in the prior subsection on modeling kinematics have applied feed-forward control to validate their models on FSIRs [41,53,61,118,125]. These studies incorporated their developed IK models into the robot's feed-forward control system and assessed performance through trajectory tracking experiments. Most validation experiments were conducted in free-space [41,53,99,101,102,109,113] because the learned IK models do not account for environmental perturbations. This limitation was addressed by [126], which collected training data both with and without obstacles to train the ANN, enhancing efficiency in specific scenarios where the difference in obstacle placement between training and testing is minimal. However, extending this method to broader applications significantly increases the need for data collection.

Compared to traditional feed-forward control relying on analytical models, the data-driven approach is simpler to implement. ML methods require only the collection of data on the FSIRs, without necessitating a comprehensive understanding of the system's intricacies. The collected data typically encompasses numerous patterns and information that ML can learn simultaneously. In contrast, analytical models demand a thorough system understanding, making them more cumbersome to adapt if the FSIRs's structure or configuration changes. Additionally, some factors might be overlooked by analytical models due to their non-observability, yet their omission can significantly affect control accuracy.

4.3.2. Feedback control

Analytical or learning-based models for feedforward control may provide sufficient accuracy for robotic systems operating in open space. However, their effectiveness diminishes when the robots encounter external disturbances or interact with the environment, leading to increased errors. Consequently, relying exclusively on feedforward control does not facilitate precise control of FSIRs. Incorporating feedback information about the robot's current state is crucial for adjusting control commands to achieve more accurate control.

Visual feedback

Visual feedback from camera offers valuable spatial information for controlling FSIRs. The camera can be integrated into the distal end of robots or positioned in the environment to monitor the procedure. However, as discussed in Section 4.1, external cameras face challenges with the line-of-sight issue, making them impractical in clinical settings. The controller uses visual feedback to estimate the discrepancy between the current and desired statuses, then adjusts the actuators to minimize this gap. For many MIPs, embedding a camera at the tip of an FSIRs is a prevalent approach, although it is not suitable for cardiac interventions due to the possibility of the camera being obscured by blood.

Li et al. introduced the use of RNN in their visual servoing control scheme, utilizing quadratic programming to manage a flexible endoscope within kinematic and physical constraints [90,91]. The RNN serves as a solver with a finite convergence time, providing a kinematic model apt for closed-loop control. This visual servoing control scheme, enhanced by accelerated RNN, was tested in two robotic platform simulations. The outcomes demonstrated that errors were below 0.2 mm, and the average computation time for each timestep was under 0.01 seconds.

Besides the potential of visual servoing via RNN, the strong capability of CNNs for extracting information from images is promising for assisting with FSIRs control. Authors in [62,127] proposed DL-based approaches to estimate the pose of a distal camera on the tip of interventional tools. They demonstrated its potential application in FSIRs control, which was later realized in a study on robotic fetoscopy by Ahmad et al. [63]. In [63], a trained CNN is used to predict the relative orientation of the placental surface from fetoscopy images. The CNN is integrated into a shared control system consisting of autonomous control of the flexible distal tip and manual gross motion control by the operator. The automatic tip control achieved a RMS error of 5.93°. Lazo et al. developed a method using CNNs, designed to autonomously navigate a robot to the central position within the lumen, regardless of its initial location [128]. Moreover, Zhao et al. utilized a CNN trained on surgical images to predict action probabilities for control [103]. To enhance the safety of MIPs, they also trained a second 1D CNN with operating forces to recognize force modes. Another approach to identifying force states in the closed-loop control of a robotic catheter is described in [122], where CNN-based identifiers for force and torque states were implemented to generate the probability of an abnormal state for catheter control. This method reduced the average operating force and torque by 20.80% and 14.20%, respectively. Owing to CNN's

Table 6
Applications of ML algorithms in the control task (yellow for traditional ML, green for DL and purple for RL).

Subtask	Reference	Involved ML Method	Actuation Method	Type of Robot	DoF	ML Role	Real-world Experiment	Simulated Experiment	Validation task	Results
Feed-forward Control using models	[101]	BNN	Cable-driven	multi-joint	7	Learn the IK to predict control signals	✓	✓	Predict tip position and motor torques	Test RMSE: [0.109, 0.145, 0.108] mm (kinematics); [0.037, 0.046, 0.050, 0.023, 0.022] Nm (dynamics)
	[109]	MLP	Cable-driven	multi-joint	7	Learn the IK to predict control signals	✓	×	Predict the trajectory	RMSE: 3.047e−07
	[102]	LSTM	Cable-driven	multi-joint	7	Learn the IK to predict control signals	✓	×	2D trajectories following	Mean tracking error norm: 3.47 mm (square trajectories)
	[53] [41]	GMM, KNNR, ELM	Cable-driven	CR	3	Learn the IK to predict control signals	✓	×	2D trajectories following	RMSE: 2.5556 mm (GMR), 2.1527 mm (KNNR), 2.3277 mm (ELM)
	[99]	ELM	Cable-driven	CR	3	Learn the IK with hysteresis to predict control signals	✓	×	2D 3D trajectories following	RMSE: 0.55 mm (2D), 2.03 mm (3D)
	[113]	PoWER	Cable-driven	CR	3	Learn the IK with nonlinearity to predict control signals	✓	✓	2D trajectories following	RMSE after RL refinement: 1.101 mm
Feedback Control	[90], [91]	RNN	Cable-driven	multi-joint	4[90], 6[91]	Quadratic programming solver for the kinematics-based control	×[90], ✓[91]	✓	Visual servoing	Error on 3 axes: < 0.2 mm; average computing time < 0.01 s [90]; Demonstrated the visual servo control [91]
	[63]	CNN	Fluidics-driven	CR	5	Predict the relative orientation of the placental surface for tip position control	✓	×	Distal tip alignment	RMSE: 5.93°
	[103]	CNN	/	Guidewire	2	Recognize the operating force mode for force control	✓	×	Obstacle avoiding	Maximum operating forces: 0.24 to 0.79 N
	[122]	CNN	/	/	/	Predict risk probability from force state and torque state	✓	×	Guidewire cannulation	Average operating force and average operating torque reduced by 20.80% and 14.20%
	[96]	LWPR	Fluidics-driven	CR	2	Learn the IK to predict control signals	✓	×	3D trajector following	Mean accuracy: ±2.21° and maximum ±7.49° ; ±2.49° and maximum ±11.03° with external disturbance
	[52]	GMM	Cable-driven	Commercial catheter	3	Learn the IK to predict control signals	✓	✓	3D trajector following	RMSE and standard deviation: 1.379±0.637 mm in reality; 1.909±1.067 mm in simulation
	[54]	SVM, MLP[a]	Cable-driven	Tendon-sheath Mechanism	2	Learn the IK to predict control signals	✓	×	2D trajectories following	Average RMS error: 0.49±0.32 and 0.62±0.36 mm for the slow and fast speeds
Control with Reinforcement Learning	[123]	SARSA	DC motors	multi-joint	1	Learn to generate policy to move the robot in colon	✓	×	In-vivo colon endoscope	RL gave significant better results in over 50% colons compared with fixed input
	[98]	MA fuzzy Q-learning	Cable-driven	Concentric tube	2, 3[b]	Learn optimal policy of each controller	×	✓	Trajectory tracking	Correlations between achieved and desired trajectories in xand Y directions: 95% and 97% (2DOF); 94% and 97% (3DOF)
	[46]	DQN	Cable-driven	Commercial catheter	3	Learn to generate policy to control the catheter	✓	✓	Reaching targets	Average distance between catheter tip and target: 4.70±1.59 mm
	[74]	DDPG	Cable-driven	Concentric tube	4, 6, 8[b]	Learn the control policy for concentric tube robots	×	✓	Trajectory following	Mean error from 0.31–4.35 mm for different types of robots tracking 3 trajectories.
	[124]	DDPG	/	Concentric tube	6	Learn the control policy for concentric tube robots	×	✓	Trajectory following	Mean Cartesian error: 1.29 mm mean Cartesian error in the IK evaluation; mean tracking error: 1.37 mm (with noise)
	[97]	DQN	Cable-driven	Commercial catheter	4	Learn the control policy for concentric tube robots	×	✓	Point tracking	RMSE: 0.003±0.0058 mm

[a] Both SVM and MLP play essential roles in [54]. For the convenience of illustration, in this table, cells of [54] are filled with yellow (traditional ML).

[b] Experiments are conducted on robots with different DOFs.

remarkable ability to effectively process various types of data, including images and force/torque measurements, CNNs have become a popular algorithm and appeared in around 10% of the reviewed articles, as shown in Fig. 4a.

Traditional ML methods have also been applied to visual feedback control, as seen in [52], where closed-loop positional control is enhanced with a novel IK model informed by visual cues. This model, developed through a dynamic GMM, was validated on 3D square trajectories, achieving a mean RMSE of 1.379 ±0.637 mm.

Electromagnetic feedback

Electromagnetic Tracking system (EMT) is widely used in FSIRs due to small size of the probe, which facilitate integration at the FSIRs tip. EMT directly provide 3D spatial information, making it often utilized to measure the position and orientation of the FSIRs tip [54,118,129]. Different ML approaches are incorporated at various stages of the FSIRs control schema. In [54], Jolaei et al. developed a learning-based kinematic control framework for soft tendon-driven catheters. A SVM algorithm classifies which tendon to drive, and the SVM classification results are then used by four deep ANNs to determine the desired length of each tendon. In trajectory following experiments, the system's average RMS error was 0.49±0.32 mm and 0.62±0.36 mm for slow and fast speeds, respectively. Position control is leveraged to facilitate force control, enabling safer catheter steering. Wu et al. introduced a DL method that reduces the contact force between the catheter and its surrounding environment [118,130]. This method relies solely on tip location measurements provided by the EMT, eliminating the need for a force sensor at the catheter tip.

4.3.3. Control with reinforcement learning

RL is frequently used to enable robotic systems to find optimal control policies while interacting with complex environments. In FSIRs

control, RL has long been a focus of research interest. With the evolution of RL, the algorithms applied in FSIRs have shifted from basic approaches like Q-learning and SARSA (state–action–reward–state–action) to more advanced, ANN-enhanced algorithms such as DQN and DDPG.

An early study by [123] employed Q-learning and SARSA to adjust the input voltage of motors, determining the speed and direction of a colon endoscope robot. A positive reward was given for forward movement of the robot, while penalties were applied to prevent undesired states, such as when torque values become very high, potentially causing the colon to contort. These methods were tested on six in-vitro colons, and both algorithms performed better in over 50% of the cases compared to the traditionally used constant velocity controller.

RL control of robots is typically approached as a single-agent-environment interaction. However, [98] redefined the control of tendon-driven manipulators as a multi-agent reinforcement learning (MARL) problem. In [98], the degrees of freedom (DoF) are considered equivalent to the number of RL agents. They employed a multi-agent fuzzy Q-learning algorithm, capable of learning the mapping between tip positions and the desired trajectory. In their simulation-based trajectory following experiments, the correlation between achieved and desired trajectories exceeded 94% for both 2 DoF and 3 DoF manipulators.

As discussed in Sections 4.1 and 4.2, ANN has emerged as one of the most utilized approaches in various FSIRs tasks, such as perception and modeling. Similarly, advancements in DRL, leveraging the development of ANN, have expanded the range of RL's applicability in the FSIRs domain. These algorithms are adept at learning complex MIP tasks using the clinical data typically available during procedures. However, the significant increase in computational resources required to train DRL agents has become a bottleneck for further application.

You et al. employed a dueling DQN algorithm to learn control of a cardiac ablation catheter tip within a simulated environment [46]. Training incorporated both angiographic images and position data. To bridge the gap between simulation and reality, random noises were introduced during training to enhance control accuracy under real-world experimental conditions. The RL agent achieved an average error of 4.70±1.59 mm between the catheter tip and the target. In research conducted by [131], an autonomous controller was developed using DRL for gentle navigation within a two-dimensional simulation of an aortic arch. This controller significantly reduced the maximum and mean contact force exerted on the vessel walls by 43% and 29%, respectively. This approach was further validated using a porcine liver model in a subsequent study [132], showcasing the autonomously trained controller's ability to learn human-like behaviors, such as rotating the guidewire tip clockwise and counterclockwise, without training on data generated by physicians.

Iyengar et al. explored the role of additional noise in RL-based control for CTR, focusing on its impact on exploration [74]. Three types of noise and CTR configurations (2-tube, 3-tube, and 4-tube) were examined with the selected RL algorithm, DDPG, which was used to generate the optimal control policy. This RL-based IK controller achieved an average extension error of 0.44 mm and a rotation error of 0.3°. In a follow-up study, the authors of [124] also utilized DDPG to develop a model-free IK solver for concentric robot control. Compared to [74], [124] dealt with a longer concentric tube and a more complex model in simulation. Moreover, a goal-based curriculum function was used to reduce training time. The proposed IK solver attained a 1.29 mm mean Cartesian error in IK evaluation, and a 1.37 mm mean tracking error in a noise-induced simulation.

In another study [97], a DRL-based approach is utilized to adapt the PID control gains as the robotic catheter interacts with its environment. A DQN, enhanced by LSTM, is employed to learn the tuning policies. This method uses a temporal learning approach to improve sampling efficiency and update the target network of the DQN between episodes. The approach is validated through a simulation experiment aimed at estimating axial displacements, achieving an RMS error of 0.003 ±0.0058 mm, which surpasses other methods(i.e., Ziegler–Nichols system and adaptive fuzzy tuning). A reinforcement learning strategy was adopted in [133] with the objective of learning to mitigate the repulsive force between the vessel wall and the catheter. This strategy aims to minimize negative impacts, including vessel perforation, thereby enhancing the safety and effectiveness of catheter navigation.

4.4. Navigation

Navigation represents a critical phase in medical procedures, where the interventional tool advances through body lumens or vessels to reach deeper sections of anatomy [10]. Manual navigation often demands significant concentration from clinicians during device deployment, while FSIRs with a higher level of autonomy in navigation can save clinicians' energy from focusing on meticulous operations during the navigation phase. This allows clinicians to focus more on crucial tasks after reaching the intervention site. Nevertheless, autonomous navigation for FSIRs is challenging because the environments are deformable and dynamic.

As a high-level task, navigation can benefit from efficient perception, reliable modeling, and precise control. Therefore, some research work on navigation has partially discussed above topics as well. In this subsection, we mainly focus on one of the most common navigation tasks, namely motion planning. Studies in other robotic domains also indicate that one of the first steps towards autonomous navigation is implementing motion planning techniques [144]. Motion planning refers to finding feasible trajectories or actions traversing the area between a starting state and a goal state while bypassing obstacles and avoiding unwanted zones. As for MIPs with FSIRs, the kinematic and geometric limitations of FSIRs also bring constraints to the planning task.

Table 7 summarizes the publications using ML techniques in the navigation task. As shown in Table 7, ML applications for FSIRs's motion planning are categorized into three broad techniques: Learning from Demonstration (LfD), RL, and computer-vision-based approaches for assisting motion planning. Among different ML algorithms appearing in the navigation task, the GMM-GMR approach is dominant, as indicated in Fig. 4b. It is mainly used in the LfD paradigm for motion planning because of its capability to encode the statistical characteristics from noisy demonstration data, and make predictions of robotic motions continuously over time. From Fig. 4b, when it comes to RL approaches, both value-based approaches (e.g., DQN) along with policy-based approaches (e.g.,DDPG), are popular in practice. In the following, each of these methods is described referring to their three categories.

4.4.1. LfD-based navigation

One of the ML approaches commonly adopted to learn human-like gestures is the LfD paradigm. In LfD, expert demonstrations are used to generate a feasible task space to automate medical navigation. Statistical models such as GMM and HMM are often adopted to encode the demonstration data, which can be recorded from distal and proximal sensors embedded in the FSIRs during manual navigation. Fitted models can work as a motion planner for FSIRs navigation. The GMM-GMR approach, which is explained in Section 2.2, is the most commonly used approach according to Table 7. The Expectation Maximization (EM) algorithm is often used to optimize the parameters of GMMs.

Rafii-Tari et al. proposed a learning-based approach for generating motion trajectories from multiple demonstrations of a catheterization task [31]. The two-DoF linear and rotational motions produced by experts at the proximal end of a catheter are recorded during the catheterization procedure. The demonstration is then modeled with GMM. Then GMR is derived from the GMM and is applied to generate optimum motion trajectories for a robotic catheter driver. This method is able to provide assistance to inexperienced operators. The proposed

Table 7
Applications of machine learning in the navigation task (yellow for traditional ML, green for DL and purple for RL).

Method	Reference	Specific Algorithm	Type of Interventions	Model Input	Model Output	Local Motion Planning	Trajectory Optimization	Learning Motion Primitives	Kinematics Constraints	Real-world Experiment	Simulated Experiment
LfD	[31]	GMM(EM)-GMR	Endovascular catheterization	Proximal data from expert motion	Motions	×	×	✓	×	✓	×
	[29]	HMM(EM)	Endovascular catheterization	Proximal data from expert motion	Motions	×	×	✓	✓	✓	×
	[95]	DMPs	Endovascular catheterization	Proximal and distal data from expert motion	Trajectories	×	✓	✓	✓	✓	×
	[23]	GMM(EM)-GMR	Endovascular catheterization	Proximal and distal data from expert motion	Trajectories	×	✓	✓	×	✓	×
	[28]	GAIL	Endovascular catheterization	Catheter states, manipulator motions	Motions	✓	×	✓	×	✓	×
	[134]	GAIL	Neurosurgery	Needle states	Trajectories	✓	✓	✓	✓	×	✓
	[27]	GMM-GMR	Laparoscopy	Tip trajectories from expert	Trajectories	×	✓	✓	✓	×	✓
	[135]	DP-Means	Laparoscopy	Tip trajectories from expert	Trajectories	×	✓	✓	✓	×	✓
	[21]	GMM-GMR	MIS	Demonstrated trajectories	Executable paths	×	✓	×	✓	✓	×
	[136]	GMM-GMR	MIS	Demonstrated trajectories	Motor trajectories	×	×	✓	×	✓	×
	[51]	GMM-GMR	Keyhole surgery	Demonstrated trajectories	Executable paths	×	✓	×	✓	✓	×
	[106], [22]	GMM-GMR	Laparoscopy	Contexts/phases of the task	Motions	×	×	✓	✓	×	✓
	[137], [106]	GMM-GMR	Laparoscopy	Octopus movements	Motions	×	×	✓	✓	×	✓
RL	[138]	Q-learning	Endovascular catheterization	2D mesh	Motions	✓	×	×	×	×	✓
	[75]	DQN, DDPG	Endovascular catheterization	Reward function	Motions	✓	×	×	×	✓	✓
	[139]	DDPG	Endovascular catheterization	Catheter states (positions) of current and past, motions of past	Motions	✓	×	×	×	✓	✓
	[140]	DQN	Transoral endotracheal	Simulated images	Motions	✓	×	×	×	×	✓
	[46]	DQN	Endovascular catheterization	Position data and video	Motions	✓	×	×	×	✓	✓
	[45]	GA3C	Neurosurgery	MRI images	Trajectories	×	✓	×	✓	×	✓
	[17]	DQN	Endovascular catheterization	Motion control commands from demonstrations	Motions	✓	×	×	×	✓	×
	[141]	MDP	Flexible needle insertion	CT images	Trajectories	×	✓	×	×	✓	✓
	[30]	UDQL	Flexible needle insertion	CT images	Trajectories	×	✓	×	×	✓	✓
	[142]	DQN	Flexible needle insertion	CT images	Trajectories	×	✓	×	×	×	✓
	[143]	A3C	Endovascular catheterization	Aortic arch model	Trajectories	×	✓	×	×	×	✓
Others	[55]	K-means and SVM	Intracardiac catheterization	Images from tip camera	Type of tissue	✓	×	×	✓	✓	✓
	[62,104]	CNN	Bronchoscopy in the lungs	Simulated images	Airway characteristics	×	×	×	×	✓	✓
	[103]	CNN	Endovascular catheterization	Motions, operating force, simulated X-ray images	(Probability of) motions	✓	×	×	×	✓	×

collaborative scheme comprises manual guidewire manipulation by the operator and automated catheter movements by the robot in a cooperative phase-by-phase manner. The same authors also proposed another cooperative framework for robotic endovascular catheterization using HMM [29]. They extended their LfD approach by decomposing the procedure into a set of primitive motions and learned the model of each primitive using HMMs. The higher-level structure of the target task is learned by a higher abstraction level HMM. The trained models are applied to generate a sequence of motions, detect operator input and predict future movements. The predicted movements during catheter navigation are displayed in a supervision interface. From the interface, the operator monitors the current and the generated following motion of the robot, and decides whether to correct the motion.

However, anatomies of different patients could vary in terms of anatomical dimensions and relative positioning, which is not considered in previously discussed works [29,31], but studied in a subsequent study [23]. This work applied a non-rigid registration method to find the warping function that maps demonstration trajectories to other anatomical models. The robot trajectories are generated by the learned motion model from the remapped trajectories. The proposed trajectory optimization and navigation method are verified in both in-silico and ex-vivo experiments.

The authors of [95] exploited a model-free algorithm, i.e., policy improvement with path integrals, for motion trajectory optimization. Human demonstrations of endovascular catheterization with a 2-DOF catheter and a 1-DOF guidewire are collected and modeled by Dynamical Movement Primitives (DMPs). DMPs are then used to initialize the policy for training. Compared with manual operation, the obtained agent improved path length, speed, maximum acceleration and distance between catheter tip motion trajectories and vessel centerlines. This method leads to less contact force than manual and robot-assisted operations without LfD.

As a related study of [23,31,95], Chi et al. [28] proposed Generative Adversarial Imitation Learning (GAIL) to achieve an automated robot-assisted endovascular catheterization on two major branches of the aortic arch, namely the brachiocephalic artery (BCA) and left common carotid artery (LCCA). GAIL is trained from expert demonstration and generates the policy for BCA cannulation. The generated policy from GAIL is reused and refined by Proximal Policy Optimization (PPO) for LCCA cannulation. The proposed agent's cannulation success rate is 94.4% on BCA and 88.9% on LCCA. Another work [145] also chose GAIL to train a steerable catheter in a 3D neurosurgical simulator. Its results demonstrate that the GAIL method is fast and can securely steer flexible catheters with high accuracy and robustness. In their later paper [134], similar to [28], PPO is combined with GAIL to

provide intra-operative path planning for motion control. Based on this approach, they proposed a path planning framework for steerable needles used in neurosurgery. This framework can achieve an average targeting error of 1.34 mm in position and 3.16 degrees in orientation in simulation. Building upon similar methodologies, the Curriculum Generative Adversarial Imitation Learning (C-GAIL) approach, a sophisticated learning from demonstration method, has been utilized to create navigation paths for robotic catheters during endovascular interventions. A distinctive aspect of C-GAIL is its consideration of the dynamic interactions between steerable catheters and vessel walls, along with the vessels' deformable characteristics. This path planning algorithm's effectiveness was demonstrated through trajectory following experiments, as detailed in [146] and [147]. Zhang et al. employed GAIL to identify the optimized pre-operative path for structural intervention cardiology [148]. The in-vitro experiments demonstrated an average tracking error of approximately 1 mm in the x, y, and z directions.

The work in [27] proposed an algorithm using the LfD paradigm to learn the feasible trajectories for a soft flexible robot. The learned information is encoded by GMM and could be extracted as possible trajectories by GMR. The variability of learned trajectories helps to keep the tip moving along the optimal trajectory while adjusting the robot shape in case of unexpected collisions with organs. In their later study [135], by introducing Dirichlet Process(DP)-Means algorithm for online clustering, the proposed approach is extended into an online learning algorithm that produces a statistical model of the natural movements of the surgeon during the task and determines a controller in the null space.

Another two works [21,136] also took a similar LfD approach with GMM-GMR as what did in [27,31] to learn the trajectories of the tendon-driven serpentine manipulator. In [21], the GMM-GMR approach is used to learn the reaching and targeting skills from the human demonstrations and plan motion trajectories for an IK-based controller to reproduce behaviors automatically. However, Xu et al. proposed to learn the motor commands directly without relying on an IK model [136]. In addition, results from GMR are used as labeled training data for Locally Weighted Regression to retrieve task-specific models for online control. GMM-GMR approach is also applied on a multiple-segment flexible robots, as shown in [51]. Similar to [21], in [51], GMM-GMR is only supposed to produce the executable trajectories, while the control is based on the analytical kinematics model of the robot.

For a surgical robot called STIFF-FLOP, a control scheme is designed by learning context-reward mapping from demonstration with the help of GMM-GMR. Then the GMM-GMR was used to refine a context-action mapping by EM [22,106]. Besides standard experiments on tip steering, an experiment mimicking a surgical scenario is performed by the robot. In this experiment, the surgeon is in charge of the tip steering while the robot is controlled to move its body around a spherical space. This experiment displayed its ability to exploit the robot kinematic redundancy and avoid the defined area. Follow-up studies [137] used a similar approach. They proposed to transfer skills from octopus motions to a STIFF-FLOP robot. Motion primitives are extracted from octopus' movements and modeled by GMM, and mapped to the STIFF-FLOP robot by GMR. They also designed a self-refinement algorithm to optimize GMM parameters based on iterative reward-weighted regression rather than the common EM-based approach.

4.4.2. RL-based navigation

In RL, an agent learns to maximize a specific reward function by taking actions and observing the interaction with the environment. Researchers adopted RL algorithms to tackle endovascular navigation in model-free approaches. Model-free approaches are commonly used RL methods that can be widely applied to different environments since they learn the optimal policy without estimating the dynamics of the environment [149]. A RL algorithm is proposed in [138] based on Q-learning to achieve navigation with a robotic catheter on two different simulated 2D aorta meshes. The learned navigation policy on the first mesh is used as a policy initialization for the second mesh.

Navigation is also performed with DRL, which benefits from the capability of ANN. An application of DQN [46] in cardiovascular intervention is already introduced in Section 4.3, and the navigation experiment is a showcase for their proposed control algorithm. A high success rate of 87% for the translation from a simulator to a real robotic system is reported in [46]. Other studies for coronary intervention are presented in [17,150]. In [17], a guidewire navigation framework for coronary interventions is proposed based on a DRL algorithm Rainbow [151], which improves DQN by combining multiple techniques. The authors also made improvements by optimizing the replay memory of DQN, setting a focus window, and utilizing segment-wise training and transfer learning. The framework was validated with a 2D coronary phantom and a 3D artery phantom with fluid flow. The final success rate of the guidewire navigation to the main target is 98% in both 2D and 3D phantoms. The DQN introduced in [150] is employed from stable RL implementations as described in [152]. Meng et al. implemented a DRL algorithm, namely Asynchronous Advantage Actor Critic (A3C), to learn the autonomous navigation into a virtual model of the aortic arch [143,153]. The in-silico experimental results demonstrated that the automatic insertion has shorter operation time and less contact force, compared with manual operation.

Cho et al. [154] proposed an approach that combines between behavior cloning and DDPG for navigating a guidewire within blood vessels. This integrated approach proved advantageous by significantly reducing the required training time. In [75], the authors compared the performance of robotic catheter navigation via two DRL approaches, DQN and DDPG, and explored the different converging speeds of several DDPG variations while training in the simulated environment. However, the robustness is still doubtful considering the simplicity of the test bench. Later in [139], they navigated a guidewire in a rigid two-dimensional vascular phantom, which is more complex and closer to the geometries of human vessels, compared with their previous work. DDPG with hindsight experience replay controls the guidewire and is trained in the simulation environment. The agent takes current and past catheter states (tip positions) and previous motions as input and outputs the next-step motion consisting of translation and rotation commands.

Works emerging with RL methods in other clinical applications are studied as well. A navigation policy based on DQN that utilizes images from a monocular camera mounted on the tip of a snake robot for tracheotomy is developed in [140]. The system is said to serve as an assistive device for clinicians to perform endoscopic intubation with minimal human input.

Besides applying catheters or concentric tubes working in the lumen, RL has also been applied to flexible needle insertion. In [30], the path planning and motion planning for steerable needles are conducted in a human-supervised way using Universal Distributional Q-learning (UDQL) to learn the steering policy. The UDQL agent is trained in simulated 2D and 3D environments, and can perform multi-target insertions through one single insertion point with the help of hindsight experience replay. The model could output a value distribution showing the risks. Experts could update the model based on their evaluation of value distribution manually to perform transfer learning. The proposed approach performed better than the deep double Q-learning network, which is a variant of DQN, in terms of steering accuracy and avoidance probability. In their previous work [141], which is not based on RL but on MDP, they proposed a robust path planning algorithm to provide secure and optimal motion planning. The steering problem is formulated in an MDP approach considering uncertainties as variables following unknown distributions. The proposed method outperforms the traditional MDPs in success rate and avoidance probability. In [142], the authors used DQN to learn a 2-DOF flexible needle insertion. Rewards are set by the distance between the target and needle tip, and a penalty is set for unexpected collision with other tissues. The GPU-based A3C algorithm (GA3C) is also applied to plan paths for a steerable

needle in [45]. It provides the optimal trajectories in terms of obstacle clearance and kinematic constraints. The results showed state-of-the-art performances in terms of obstacle avoidance, trajectory smoothness and computational time. Kumar et al. [155] utilized DDPG model to generate paths for flexible needles in keyhole neurosurgery. The results of the in-silico experiments demonstrated that the DDPG model outperformed the RRT* algorithm by producing trajectories that were both smoother and shorter. Hu et al. [156] proposed a Double Deep Q-learning Network (DDQN) for obtaining the optimal path for flexible needle puncture. The DDQN method represents an enhancement over the traditional DQN by exhibiting superior learning efficiency.

4.4.3. Other methods

In many clinical scenarios, a camera is attached at the distal end of the flexible robots, sending back real-time visual information of the current state. Navigation could be achieved by utilizing visual feedback. These methods are classified as computer vision-based navigation.

Fagogenis et al. proposed a wall-following algorithm for navigation using only visual guidance [55]. K-means and SVM classifiers for images are fully trained on a small set of images. The obtained classifiers can distinguish between blood or ventricular walls and the bioprosthetic aortic valve. Depending on the type of tissue that the FSIRs is contacting, they can switch between two navigation modes to complete complex clinical tasks.

Besides SVM classifiers, ANNs, especially CNNs, are also widely used in visual guidance for FSIRs navigation. Developments in CNN architectures have enabled the real-time localization of the bronchoscope using video from a distal end camera. This advancement has facilitated the implementation of closed-loop control systems with visual guidance, as demonstrated in the studies conducted by Sganga et al. [62,104]. The CNNs are trained to produce features of visible airways, which are then fed to the motion controller of the robotic bronchoscope to generate the desired trajectory from a list of planned airways. With the proposed navigation method, the robot successfully reached the target in the lung in 19 out of 20 trials. Another DL approach utilizing CNNs to navigate an endovascular robot makes use of images of the current clinical state from X-rays. In [103], Zhao et al. proposed a CNN-based framework that considers both simulated X-ray images from an external camera and internal operating force to make decisions collaboratively during navigation. Demonstration data consisting of operating actions, operating force, and medical state images are collected to train two CNNs: a 2D CNN trained by medical images to predict action probability and a 1D CNN trained by operating forces to recognize the force mode. This navigation framework achieved a success rate above 84% on a mixture of data from two cases.

5. Discussions

The ML approaches have been successfully applied in FSIRs tasks involving perception [20,82,85], modeling [40,41,53,66], control [52,90,98,103], and semi-autonomous/autonomous navigation [23,28,31,55]. Fig. 5a reflects the frequency of papers related to FSIRs using ML techniques by year, showing a steady increase with a peak in 2019. Furthermore, the areas where ML methods are most commonly applied are control and navigation. Fig. 5b summarizes the exploitations for the four categories of ML approaches. The usage of traditional ML algorithms is observed to vary from year to year, maintaining a stable presence from 2013 to 2020. However, after 2020, the frequency of use of traditional ML methods began to decline. This stable presence of traditional ML techniques may be related to the fact that traditional ML approaches remain the most suitable choices when working with small datasets, which are very common in the FSIR context, where DL techniques cannot be trained effectively. The application of DL has experienced rapid growth since 2017, a trend that has persisted through 2022. This growth aligns with trends in other scientific fields and is attributed to the DL boom initiated by AlphaGo in 2016. In addition, the increased accessibility of open source DL libraries (e.g., Tensorflow, first released in November 2015, and Pytorch, first released in September 2016) has fed this booming trend. As can be seen in Fig. 5b, the use of RL have also increased from 2017 onward. Since 2017, 20 out of 27 RL-relevant articles have utilized DL techniques. The DRL has benefited from the growth in ANN. Despite the aforementioned growth in popularity, applying various ML methods to FSIRs still encounters some common limitations and challenges. We aim to discuss these common hindrances, as identified in the reviewed literature, along with some open issues that have not been frequently mentioned in recent research.

Performance gaps among in-silico, in-vitro experiment and in-vivo test

A well-accepted procedure for validating algorithms on medical robots involves initially testing the robotic functionality in computer-based simulators and bench-top synthetic phantoms before conducting in-vivo animal or human trials [46,61,89]. This step is crucial for clinical applications, where safety, ethical, and legal guidelines must be considered.

However, the discrepancies between simulated and *in-vitro* environments, often referred to as the "reality gap," can lead to shortcomings or performance decay when an ML model trained on simulated data is deployed in a bench-top environment. These differences stem from modeling errors, as it is highly challenging to accurately model contact forces, friction, tool-tissue interaction, sensor noise, and lighting conditions. These challenges contribute to the performance decay of ML methods when the training and testing environments differ. Consequently, creating surgical simulations has become a widely studied topic in the literature, necessitating realistic and real-time modeling of soft tissue responses to tool-tissue interactions, as well as realistic rendering [157].

Various studies have attempted to solve the reality gap by introducing perturbances in the environment or focus on domain randomization [158]. Domain randomization techniques try to generate large volumes of simulation data by considering the sim-to-real differences in a virtual environment [159,160]. In the reviewed works of FSIRs, randomized noises are added to the simulation environment, so as to make the simulated experiment more complicated and realistic [27,46,74,95]. Another solution is generating synthetic data that are close to real data. Some recent works have used Generative Adversarial Networks (GANs) to construct a mapping between simulated and real domains, then to create synthetic data, such as [111,161,162].

One can expect that another gap exists between bench-top and in-vivo experiments. Here, bench-top experiments refer to those using either synthetic phantoms or ex-vivo tissues. This gap has been less reported, partly because there have been few studies applying ML techniques in in-vivo experiments [55,123]. In-vivo environments are considered more complicated due to the robot's interaction with various body fluids and soft tissues. Another challenge arises from physiological movements, such as breathing and heartbeat, which render in-vivo environments dynamic. Thus, maintaining precise control of robots is more challenging in in-vivo settings.

Limited interpretability of ML algorithms

In Section 1 and Section 2, the interpretability of ML and some interpretable ML models are described. However, the limited interpretability of the ML algorithms are not yet discussed. Interpretability is defined as *"the degree to which a human can understand the cause of a decision"* [163]. A ML model characterized by a straightforward mathematical or statistical expression, such as a linear regression model, typically offers enhanced comprehensibility regarding its predictive or decision-making processes. In contrast, this level of interpretability is often not present in more complex models such as ANN, where the intricate interplay of numerous parameters and non-linear transformations makes the

rationale behind predictions or decisions less transparent. The limited interpretability of ANN raises safety concerns on the application of this technique on FSIRs. ANN is often viewed as a "black-box" because it is difficult for a human to follow the data stream from the raw input to the network output. In addition, the knowledge that ANN learns is stored in hidden layers. The parameters of an ANN such as weights and biases that a human can directly observe do not contain any physical meaning. This information are thus too complex for a human to interpret. Therefore, the use of ANN with FSIRs may raise doubts on reliability and acceptability issues for clinicians.

The growing interest in Explainable AI (XAI) [164] reflects a trend towards enhancing model interpretability. One could use inherently interpretable models such as Linear Regression or Decision Trees [163] as their mathematical foundations are clear and some of their parameters have direct physical meanings that are easily relatable to the features in the data. An alternative approach involves employing model-agnostic interpretative techniques [165], which provide insights into the rationale behind a model's predictions. Increasingly powerful visualization methods are developed to increase the intuitiveness of understanding what happens inside the AI. For instance, t-distributed Stochastic Neighbor Embedding (t-SNE) [166] helps the data interpretation by revealing underlying patterns and relationships within the data. Partial Dependence Plots [167] and Individual Conditional Expectation Plots [168] play a crucial role in visualizing the influence of input features on predictions. Furthermore, saliency maps [169] are invaluable for interpreting ANN in vision-related tasks, as they highlight specific regions or features in the input data that significantly impact the model's output. Ablation study has also been used when applying ANNs-based algorithms on the FSIRs [60,118]. Through an ablation study, one can determine the contributions of each part in an ML algorithm to the overall performance, or justify the selection of the ANN hyperparameters. For a more comprehensive understanding of XAI methods applicable to black-box ML models, please refer to [49].

The limited interpretability of ML algorithms also increases the uncertainties of an FSIRs system. In safety-critical areas such as MIPs, it is crucial to adhere to high safety standards as errors in robotic control can lead to hazardous situations [170]. However, it is difficult to guarantee safety in all circumstances when dealing with complex computer-controlled systems such as FSIRs [171], especially when ML techniques are incorporated (even experienced surgeons or interventionists are not flawless).

Due to the uncertainties involved in ML models, providing guarantees of safe behavior in a trained model is highly challenging [172]. To mitigate the risks caused by uncertainties, recent regulatory measures in the high-risk category, such as surgical robots, are directed towards involving human supervision [170]. Hence, systems integrating ML techniques may consider including humans in the loop in earlier designing phases [170], which could further enable shared control. The human-involved shared control can be done by, e.g., visualization in real-time of the system's status or predictive display of future actions the system intends to pursue before actually executing those actions [173]. It is also possible to evaluate the risk of future actions by algorithms and manage the risk with human supervision, as implemented in [30]. Another example of shared control is that manual and autonomous control are switched in different phases of the MIPs, depending on the complexity of the tasks [31]. Moreover, some studies have proposed safe-reinforcement learning using formal verification methods for robot-assisted MIPs [174]. Other techniques for safe-reinforcement learning that have not yet been applied in the surgical domain are reviewed in [175].

Data issues

In terms of data collection, unlike image recognition or natural language processing, where huge labeled data sets are open to the public, medical data for FSIRs research, such as endoscopic images, is typically limited in size. It is often difficult for researchers to collect more clinical data from external data centers because sharing medical data still has privacy concerns. As an attractive solution to overcome the shortage of medical data, federated learning has been embraced by the medical image community. Federated learning utilizes data from individual data sites to train a global model without sharing the data directly, so as to improve the robustness and performance of the global model while protecting data privacy.

Another problem is the bias in data because surgical specialties and employed instruments may be quite dependent on the center where data was gathered. Data lacking the variability across centers may result in potentially ill-suited systems and misdiagnoses [176]. For instance, in the clinical studies of [176], excluding data of African-Americans led to the misclassification of some patients as pathogenic. In practice, to enrich training data for ML, artificially manufacturing synthetic data has been adopted in clinical studies [177]. In the context of FSIRs, synthetic data is often used to enlarge datasets with real sensor data [63,111,162]. However, creating assessment criteria for objectively evaluating synthetic data is still an open question [178].

Different vision between engineers and clinicians

Yet another problem is the difference between metrics of algorithms and clinical needs. Researchers may be excited to see ML model performance metrics improve, but this does not necessarily result in an improved clinical outcome, which matters for clinicians (and patients). From the clinicians' perspective, performance of ML algorithms may not be the most convincing factor to use ML. Sometimes the improvements in performance metrics are at the expense of changing the clinicians' customs. Clinicians may also have concerns about the applicability of ML algorithms in complex clinical applications. ML algorithms' ability to justify its outputs and help clinicians understand the output has been generally believed to be crucial to establish clinicians' trust in ML [179]. To eliminate barriers in vision, researchers have to collaborate more closely with clinicians and evaluate the results from the clinician's perspective from bench-top to in-vivo experiments.

Ethical and liability aspects

The use of ML algorithms with FSIRs is not only a problem for researchers but also requires a broader discussion from an ethical and liability viewpoint. From the ethical side, informed consent is a principle in healthcare, but it could be a challenge when ML is involved in clinical practice. As we discussed before, due to the limited interpretability of some ML algorithms, clinicians may feel hard to understand the reason for ML's outputs, let alone inform and educate the patients about the complexity of ML used by the devices. In addition, liability for ML-involved clinical devices such as FSIRs is another challenge. Who will be liable if a FSIRs with deployed ML algorithms makes a mistake? More existing ethical and legal challenges have been discussed in the larger context of AI in healthcare by [59].

6. Conclusions

This article reviews and discusses current applications and research activities of ML algorithms in the context of FSIRs. ML has played an increasingly important role in various tasks of FSIRs, such as perception, modeling, control, and navigation. From the perspective of interventional tasks, this article aims to outline the broad landscape, illustrating how different ML algorithms are becoming popular in various scenarios. This provides a clear indication of how advances in ML could enhance the application of FSIRs in clinical procedures. From the perspective of ML algorithms, readers can gain insights into the functionalities that ML can perform. This can assist researchers in selecting algorithms when considering ML as an alternative to conventional analytical methods in FSIRs tasks. Additionally, this paper describes an

analysis of the workflow among ML algorithms, clinicians, and FSIRs. Clinicians can focus on high-level tasks when working with ML-based FSIRs, while expert demonstrations may help ML algorithms learn skills from clinicians, thereby improving the level of autonomy of FSIRs. In this manner, FSIRs has the potential to become more intelligent over time with the use of ML.

Advances of autonomy in FSIRs still face challenges due to the limitations of ML and clinical factors. Much work is needed before these techniques can be used in real clinical practice. As a matter of fact, the validation of the vast majority of the works presented in this review only took place in in-vitro experiments. Also, some popular ML algorithms often behave as "black boxes", indicating that there is still a considerable journey ahead in enhancing the interpretability of ML. Data of high quality is always substantial to train ML models, yet it is not easily accessible and challenging to synthesize. Moreover, this is likely to be crucial if one wants to convince the developers but, more importantly, the clinicians to put their trust in said ML algorithms. Enhancing interpretability is also essential for building trust in ML, thereby facilitating its better utilization and the adoption of FSIRs supported by ML in clinical practice.

CRediT authorship contribution statement

Di Wu: Conceptualization, Visualization, Funding acquisition, Writing – original draft, Writing – review & editing. **Renchi Zhang:** Visualization, Writing – original draft, Writing – review & editing. **Ameya Pore:** Writing – review & editing. **Diego Dall'Alba:** Writing – review & editing. **Xuan Thao Ha:** Writing – original draft. **Zhen Li:** Writing – review & editing. **Yao Zhang:** Writing – review & editing. **Fernando Herrera:** Writing – review & editing. **Mouloud Ourak:** Writing – review & editing. **Wojtek Kowalczyk:** Writing – review & editing. **Elena De Momi:** Writing – review & editing. **Alícia Casals:** Writing – review & editing. **Jenny Dankelman:** Supervision, Writing – review & editing. **Jens Kober:** Writing – review & editing. **Arianna Menciassi:** Supervision, Writing – review & editing. **Paolo Fiorini:** Writing – review & editing. **Emmanuel Vander Poorten:** Conceptualization, Funding acquisition, Project administration, Supervision, Writing – review & editing.

Declaration of competing interest

The authors declare that they have no known competing financial interests or personal relationships that could have appeared to influence the work reported in this paper.

Data availability

No data was used for the research described in the article.

Acknowledgments

This work was supported by the ATLAS project. ATLAS received funding from the European Union's Horizon 2020 research and innovation programme under the Marie Sklodowska-Curie grant agreement No. 813782. This research is also funded by the Postdoctoral Mandates (PDM), an internal fund of KU Leuven under Project No. 3E230593. Moreover, this work has also received funding from the European Union's Horizon 2020 research and innovation programme under grant agreement No. 101017140, the ARTERY project.

References

[1] S. Khan, A. Tsung, ASO Author reflections: The evolution of minimally invasive liver surgery and the future with robotics, Ann. Surg. Oncol. 25 (3) (2018) 786–787.
[2] B. Jaffray, Minimally invasive surgery, Arch. Dis. Childhood 90 (5) (2005) 537–542.
[3] X. Hu, A. Chen, Y. Luo, C. Zhang, E. Zhang, Steerable catheters for minimally invasive surgery: a review and future directions, Comput. Assist. Surg. 23 (1) (2018) 21–41.
[4] D.B. Camarillo, et al., Mechanics modeling of tendon-driven continuum manipulators, IEEE Trans. Robot. 24 (6) (2008) 1262–1273.
[5] P.E. Dupont, et al., Design and control of concentric-tube robots, IEEE Trans. Robot. 26 (2) (2009) 209–225.
[6] R.J. Webster, A.M. Okamura, N.J. Cowan, Toward active cannulas: Miniature snake-like surgical robots, in: 2006 IEEE/RSJ international conference on intelligent robots and systems, IEEE, 2006, pp. 2857–2863.
[7] P. Berthet-Rayne, et al., The i 2 snake robotic platform for endoscopic surgery, Ann. Biomed. Eng. 46 (10) (2018) 1663–1675.
[8] T. Watts, R. Secoli, F.R. y Baena, A mechanics-based model for 3-D steering of programmable bevel-tip needles, IEEE Trans. Robot. 35 (2) (2018) 371–386.
[9] J. Burgner-Kahrs, et al., Continuum robots for medical applications: A survey, IEEE Trans. Robot. 31 (6) (2015) 1261–1280.
[10] V. Vitiello, et al., Emerging robotic platforms for minimally invasive surgery, IEEE Rev. Biomed. Eng. 6 (2012) 111–126.
[11] O.M. Omisore, S. Han, J. Xiong, H. Li, Z. Li, L. Wang, A review on flexible robotic systems for minimally invasive surgery, IEEE Trans. Syst., Man, Cybern.: Syst. (2020).
[12] T. da Veiga, et al., Challenges of continuum robots in clinical context: A review, Prog. Biomed. Eng. 2 (3) (2020) 032003.
[13] F. Doglietto, et al., A brief history of endoscopic transsphenoidal surgery—from Philipp Bozzini to the First World Congress of Endoscopic Skull Base Surgery, Neurosurg. Focus 19 (6) (2005) 1–6.
[14] E.B. Rosero, et al., Sex, race, and age distributions of mean aortic wall thickness in a multiethnic population-based sample, J. Vasc. Surg. 53 (4) (2011) 950–957.
[15] S.B. Kesner, et al., Position control of motion compensation cardiac catheters, IEEE Trans. Robot. 27 (6) (2011) 1045–1055.
[16] A. Brost, R. Liao, N. Strobel, J. Hornegger, Respiratory motion compensation by model-based catheter tracking during EP procedures, Med. Image Anal. 14 (5) (2010) 695–706.
[17] J. Kweon, et al., Deep reinforcement learning for guidewire navigation in coronary artery phantom, IEEE Access 9 (2021) 166409–166422.
[18] E. Vander Poorten, et al., Cognitive autonomous catheters operating in dynamic environments, J. Med. Robot. Res. 1 (03) (2016) 1640011.
[19] G.P. Moustris, et al., Evolution of autonomous and semi-autonomous robotic surgical systems: a review of the literature, Int. J. Med. Robot. Comput. Assist. Surg. 7 (4) (2011) 375–392.
[20] S. Sefati, et al., Data-driven shape sensing of a surgical continuum manipulator using an uncalibrated fiber bragg grating sensor, IEEE Sens. J. 21 (3) (2020) 3066–3076.
[21] J. Chen, H.Y. Lau, Transferring autonomous reaching and targeting behaviors for cable-driven robots in minimally invasive surgery, in: 2016 IEEE Workshop on Advanced Robotics and Its Social Impacts, ARSO, IEEE, 2016, pp. 79–84.
[22] S. Calinon, et al., Human–robot skills transfer interfaces for a flexible surgical robot, Comput. Methods Programs Biomed. 116 (2) (2014) 81–96.
[23] W. Chi, et al., Learning-based endovascular navigation through the use of non-rigid registration for collaborative robotic catheterization, Int. J. Comput. Assist. Radiol. Surg. 13 (6) (2018) 855–864.
[24] Y. Kassahun, et al., Surgical robotics beyond enhanced dexterity instrumentation: a survey of machine learning techniques and their role in intelligent and autonomous surgical actions, Int. J. Comput. Assist. Radiol. Surg. 11 (4) (2016) 553–568.
[25] T. Panch, P. Szolovits, R. Atun, Artificial intelligence, machine learning and health systems, J. Glob. Health 8 (2) (2018).
[26] A.L. Beam, I.S. Kohane, Big data and machine learning in health care, JAMA 319 (13) (2018) 1317–1318.
[27] D. Bruno, S. Calinon, D.G. Caldwell, Null space redundancy learning for a flexible surgical robot, in: 2014 IEEE Inter. Conf. on Robot. and Automat., ICRA, IEEE, 2014, pp. 2443–2448.
[28] W. Chi, et al., Collaborative robot-assisted endovascular catheterization with generative adversarial imitation learning, in: 2020 IEEE Inter. Conf. on Robot. and Automat., ICRA, IEEE, 2020, pp. 2414–2420.
[29] H. Rafii-Tari, et al., Hierarchical HMM based learning of navigation primitives for cooperative robotic endovascular catheterization, in: Inter. Conf. on Med. Image Comput. and Comput.-Assisted Intervention, Springer, 2014, pp. 496–503.
[30] X. Tan, et al., Robot-assisted flexible needle insertion using universal distributional deep reinforcement learning, Int. J. Comput. Assist. Radiol. Surg. 15 (2) (2020) 341–349.

[31] H. Rafii-Tari, et al., Learning-based modeling of endovascular navigation for collaborative robotic catheterization, in: Int. Conf. on Med. Image Comput. and Comput.-Assisted Intervention, Springer, 2013, pp. 369–377.

[32] H. Rafii-Tari, C.J. Payne, G.-Z. Yang, Current and emerging robot-assisted endovascular catheterization technologies: a review, Ann. Biomed. Eng. 42 (4) (2014) 697–715.

[33] D. Kim, et al., Review of machine learning methods in soft robotics, PLoS One 16 (2) (2021) e0246102.

[34] R. Chrisley, Embodied artificial intelligence, Artif. Intell. 149 (1) (2003) 131–150.

[35] M.A. Boden, 4 GOFAI, in: The Cambridge Handbook of Artificial Intelligence, Cambridge University Press Cambridge, 2014, p. 89.

[36] E. Alpaydin, Introduction to Machine Learning, MIT Press, 2020.

[37] K.P. Murphy, Machine Learning: a Probabilistic Perspective, MIT Press, 2012.

[38] R.S. Sutton, A.G. Barto, Reinforcement Learning: an Introduction, MIT Press, 2018.

[39] Y. LeCun, Y. Bengio, G. Hinton, Deep learning, Nature 521 (7553) (2015) 436–444.

[40] R. Grassmann, V. Modes, J. Burgner-Kahrs, Learning the forward and inverse kinematics of a 6-DOF concentric tube continuum robot in SE (3), in: 2018 IEEE/RSJ Int. Conf. on Intell. Robots and Systems, IROS, IEEE, 2018, pp. 5125–5132.

[41] W. Xu, J. Chen, H.Y. Lau, H. Ren, Data-driven methods towards learning the highly nonlinear inverse kinematics of tendon-driven surgical manipulators, Int. J. Med. Robot. Comput. Assist. Surg. 13 (3) (2017) e1774.

[42] C. Shi, et al., Shape sensing techniques for continuum robots in minimally invasive surgery: A survey, IEEE Trans. Biomed. Eng. 64 (8) (2016) 1665–1678.

[43] J. Chen, H.Y. Lau, W. Xu, H. Ren, Towards transferring skills to flexible surgical robots with programming by demonstration and reinforcement learning, in: 2016 Eighth Int. Conf. on Adv. Comput. Intell., ICACI, IEEE, 2016, pp. 378–384.

[44] L. Li, et al., Unsupervised-learning-based continuous depth and motion estimation with monocular endoscopy for virtual reality minimally invasive surgery, IEEE Trans. Ind. Inform. 17 (6) (2020) 3920–3928.

[45] A. Segato, et al., Ga3c reinforcement learning for surgical steerable catheter path planning, in: 2020 IEEE International Conference on Robotics and Automation, ICRA, IEEE, 2020, pp. 2429–2435.

[46] H. You, et al., Automatic control of cardiac ablation catheter with deep reinforcement learning method, J. Mech. Sci. Technol. 33 (11) (2019) 5415–5423.

[47] N. O'Mahony, et al., Deep learning vs. traditional computer vision, in: Science and Information Conference, Springer, 2019, pp. 128–144.

[48] J.S. Raj, et al., Recurrent neural networks and nonlinear prediction in support vector machines, J. Soft Comput. Paradigm (JSCP) 1 (01) (2019) 33–40.

[49] R. Guidotti, et al., A survey of methods for explaining black box models, ACM comput. surv. (CSUR) 51 (5) (2018) 1–42.

[50] H.G. Sung, Gaussian Mixture Regression and Classification, Rice University, 2004.

[51] H. Wang, J. Chen, H.Y. Lau, H. Ren, Motion planning based on learning from demonstration for multiple-segment flexible soft robots actuated by electroactive polymers, IEEE Robot. Autom. Lett. 1 (1) (2016) 391–398.

[52] B. Yu, et al., Probabilistic kinematic model of a robotic catheter for 3D position control, Soft Robot. 6 (2) (2019) 184–194.

[53] J. Chen, H.Y. Lau, Learning the inverse kinematics of tendon-driven soft manipulators with K-nearest Neighbors Regression and Gaussian Mixture Regression, in: 2016 2nd Int. Conf. on Control, Automat. and Robot., ICCAR, IEEE, 2016, pp. 103–107.

[54] M. Jolaei, et al., Toward task autonomy in robotic cardiac ablation: Learning-based kinematic control of soft tendon-driven catheters, Soft Robot. 8 (3) (2021) 340–351.

[55] G. Fagogenis, et al., Autonomous robotic intracardiac catheter navigation using haptic vision, Science Robotics 4 (29) (2019) eaaw1977.

[56] D.E. Rumelhart, et al., Learning representations by back-propagating errors, Nature 323 (6088) (1986) 533–536.

[57] Y.E. Wang, G.-Y. Wei, D. Brooks, Benchmarking TPU, GPU, and CPU platforms for deep learning, 2019, arXiv preprint arXiv:1907.10701.

[58] A. Paszke, et al., Pytorch: An imperative style, high-performance deep learning library, Adv. Neural Inf. Process. Syst. 32 (2019) 8026–8037.

[59] S. Gerke, T. Minssen, G. Cohen, Ethical and legal challenges of artificial intelligence-driven healthcare, in: Artificial Intelligence in Healthcare, Elsevier, 2020, pp. 295–336.

[60] O.M. Omisore, et al., Learning-based parameter estimation for hysteresis modeling in robotic catheterization, in: 2019 41st Annual International Conference of the IEEE Engineering in Medicine and Biology Society, EMBC, IEEE, 2019, pp. 5399–5402.

[61] T.G. Thuruthel, E. Falotico, M. Cianchetti, C. Laschi, Learning global inverse kinematics solutions for a continuum robot, in: Symp. on Robot Design, Dynamics and Control, Springer, 2016, pp. 47–54.

[62] J. Sganga, et al., Autonomous driving in the lung using deep learning for localization, 2019, arXiv preprint arXiv:1907.08136.

[63] M.A. Ahmad, et al., Deep learning-based monocular placental pose estimation: towards collaborative robotics in fetoscopy, Int. J. Comput. Assist. Radiol. Surg. 15 (9) (2020) 1561–1571.

[64] X. Li, et al., Deep learning for haptic feedback of flexible endoscopic robot without prior knowledge on sheath configuration, Int. J. Mech. Sci. 163 (2019) 105129.

[65] M.Z. Alom, et al., The history began from alexnet: A comprehensive survey on deep learning approaches, 2018, arXiv preprint arXiv:1803.01164.

[66] D. Wu, et al., Hysteresis modeling of robotic catheters based on long short-term memory network for improved environment reconstruction, IEEE Robot. Automat. Lett. 6 (2) (2021) 2106–2113.

[67] X. Li, et al., Distal-end force prediction of tendon-sheath mechanisms for flexible endoscopic surgical robots using deep learning, Mech. Mach. Theory 134 (2019) 323–337.

[68] T.O. Akinyemi, O.M. Omisore, X. Chen, W. Duan, W. Du, G. Yi, L. Wang, Adapting neural-based models for position error compensation in robotic catheter systems, Appl. Sci. 12 (21) (2022) 10936.

[69] D. Silver, et al., Mastering the game of go without human knowledge, Nature 550 (7676) (2017) 354–359.

[70] D. Sliver, et al., A general reinforcement learning algorithm that masters chess, Shogi, and Go through self-play, Science 362 (6419) (2018) 1140–1144.

[71] C. Berner, et al., Dota 2 with large scale deep reinforcement learning, 2019, arXiv preprint arXiv:1912.06680.

[72] V. Mnih, et al., Human-level control through deep reinforcement learning, Nature 518 (7540) (2015) 529–533.

[73] D. Silver, et al., Deterministic policy gradient algorithms, in: Int. Conf. on Machine Learning, PMLR, 2014, pp. 387–395.

[74] K. Iyengar, et al., Investigating exploration for deep reinforcement learning of concentric tube robot control, Int. J. Comput. Assist. Radiol. Surg. 15 (7) (2020) 1157–1165.

[75] T. Behr, et al., Deep reinforcement learning for the navigation of neurovascular catheters, Curr. Direct. Biomed. Eng. 5 (1) (2019) 5–8.

[76] S. Satheeshbabu, et al., Open loop position control of soft continuum arm using deep reinforcement learning, in: 2019 Int. Conf. on Robot. and Automat., ICRA, IEEE, 2019, pp. 5133–5139.

[77] M. Schotten, et al., A brief history of Scopus: The world's largest abstract and citation database of scientific literature, in: Research Analytics, Auerbach Publications, 2017, pp. 31–58.

[78] M.E. Rose, et al., Pybliometrics: Scriptable bibliometrics using a Python interface to Scopus, SoftwareX 10 (2019) 100263.

[79] N. Ito, et al., Endoscopic diagnostic support system for cT1b colorectal cancer using deep learning, Oncology 96 (1) (2019) 44–50.

[80] P. Brandao, et al., Towards a computed-aided diagnosis system in colonoscopy: automatic polyp segmentation using convolution neural networks, J. Med. Robot. Res. 3 (02) (2018) 1840002.

[81] L. Li, et al., Unsupervised-learning-based continuous depth and motion estimation with monocular endoscopy for virtual reality minimally invasive surgery, IEEE Trans. Ind. Inform. 17 (6) (2020) 3920–3928.

[82] R.L. Truby, C. Della Santina, D. Rus, Distributed proprioception of 3D configuration in soft, sensorized robots via deep learning, IEEE Robot. Automat. Lett. 5 (2) (2020) 3299–3306.

[83] S. Manavi, et al., Using supervised deep-learning to model edge-FBG shape sensors: a feasibility study, in: Optical Sensors 2021, Vol. 11772, SPIE, 2021, pp. 79–88.

[84] X.T. Ha, et al., Shape sensing of flexible robots based on deep learning, IEEE Trans. Robot. (2022).

[85] C. Della Santina, R.L. Truby, D. Rus, Data–driven disturbance observers for estimating external forces on soft robots, IEEE Robot. Autom. Lett. 5 (4) (2020) 5717–5724.

[86] S. Sefati, et al., Learning to detect collisions for continuum manipulators without a prior model, in: Int. Conf. on Med. Image Comput. and Computer-Assisted Intervention, Springer, 2019, pp. 182–190.

[87] X.T. Ha, et al., Contact localization of continuum and flexible robot using data-driven approach, IEEE Robot. Autom. Lett. 7 (3) (2022) 6910–6917, http://dx.doi.org/10.1109/LRA.2022.3176723.

[88] X. Yu, et al., Real-time assessment of catheter contact and orientation using an integrated optical coherence tomography cardiac ablation catheter, Appl. Opt. 58 (14) (2019) 3823–3829.

[89] H. Donat, et al., Estimating tip contact forces for concentric tube continuum robots based on backbone deflection, IEEE Trans. Med. Robot. Bionics 2 (4) (2020) 619–630.

[90] W. Li, P.W.Y. Chiu, Z. Li, An accelerated finite-time convergent neural network for visual servoing of a flexible surgical endoscope with physical and RCM constraints, IEEE Trans. Neural Netw. Learn. Syst. 31 (12) (2020) 5272–5284.

[91] W. Li, et al., An accelerated recurrent neural network for visual servo control of a robotic flexible endoscope with joint limit constraint, IEEE Trans. Ind. Electron. 67 (12) (2019) 10787–10797.

[92] S. Cho, et al., Roughly collected dataset for contact force sensing catheter, 2021, arXiv preprint arXiv:2102.01932.

[93] A. Kuntz, A. Sethi, R.J. Webster, R. Alterovitz, Learning the complete shape of concentric tube robots, IEEE Trans. Med. Robot. Bionics 2 (2) (2020) 140–147.

[94] C. Watson, T.K. Morimoto, Permanent magnet-based localization for growing robots in medical applications, IEEE Robot. Autom. Lett. 5 (2) (2020) 2666–2673.
[95] W. Chi, et al., Trajectory optimization of robot-assisted endovascular catheterization with reinforcement learning, in: 2018 IEEE/RSJ International Conference on Intelligent Robots and Systems, IROS, IEEE, 2018, pp. 3875–3881.
[96] K.-H. Lee, et al., Nonparametric online learning control for soft continuum robot: An enabling technique for effective endoscopic navigation, Soft Robot. 4 (4) (2017) 324–337.
[97] O. Mumini Omisore, et al., A novel sample-efficient deep reinforcement learning with episodic policy transfer for PID-based control in cardiac catheterization robots, 2021, arXiv e-prints, arXiv–2110.
[98] M. Goharimanesh, A. Mehrkish, F. Janabi-Sharifi, A fuzzy reinforcement learning approach for continuum robot control, J. Intell. Robot. Syst. 100 (3) (2020) 809–826.
[99] R.A. Porto, F. Nageotte, P. Zanne, M. de Mathelin, Position control of medical cable-driven flexible instruments by combining machine learning and kinematic analysis, in: 2019 Int. Conf. on Robot. and Automat., ICRA, IEEE, 2019, pp. 7913–7919.
[100] W. Jiang, T. Yu, X. He, Y. Yang, Z. Wang, H. Liu, Data-driven modeling the nonlinear backlash of steerable endoscope under a large deflection cannulation in ERCP surgery, in: 2021 IEEE Int. Conf. on Real-Time Comput. and Robot., RCAR, IEEE, 2021, pp. 39–44.
[101] F. Cursi, et al., Bayesian neural network modeling and hierarchical mpc for a tendon-driven surgical robot with uncertainty minimization, IEEE Robot. Automat. Lett. 6 (2) (2021) 2642–2649.
[102] W. Bai, et al., Task-based LSTM kinematic modeling for a tendon-driven flexible surgical robot, IEEE Trans. Med. Robot. Bionics 4 (2) (2021) 339–342.
[103] Y. Zhao, et al., A CNN-based prototype method of unstructured surgical state perception and navigation for an endovascular surgery robot, Med. Biol. Eng. Comput. 57 (9) (2019) 1875–1887.
[104] J. Sganga, Autonomous Navigation of a Flexible Surgical Robot in the Lungs, Stanford University, 2019.
[105] M.S. Malekzadeh, et al., A skill transfer approach for continuum robots—imitation of octopus reaching motion with the stiff-flop robot, in: 2014 AAAI Fall Symposium Series, 2014.
[106] M.S. Malekzadeh, D. Bruno, et al., Skills transfer across dissimilar robots by learning context-dependent rewards, in: 2013 IEEE/RSJ Int. Conf. on Intell. Robots and Syst., IEEE, 2013, pp. 1746–1751.
[107] P. Yaftian, N. Bandari, J. Dargahi, A. Hooshiar, Comparison of mechanistic and learning-based tip force estimation on tendon-driven soft robotic catheters, in: 2022 44th Annual International Conference of the IEEE Engineering in Medicine & Biology Society, EMBC, IEEE, 2022, pp. 3489–3494.
[108] C. Bergeles, et al., Concentric tube robot kinematics using neural networks, in: Hamlyn Symp. on Medical Robotics, 2015, pp. 13–14.
[109] W. Li, et al., Poster: Learning-based modeling and control of micro-IGES surgical robot, in: Hamlyn Symp. on Medical Robotics, 2021.
[110] D. Baek, J.-H. Seo, J. Kim, D.-S. Kwon, Hysteresis compensator with learning-based pose estimation for a flexible endoscopic surgery robot, in: 2019 IEEE/RSJ International Conference on Intelligent Robots and Systems, IROS, IEEE, 2019, pp. 2983–2989.
[111] D. Baek, et al., Hysteresis compensator with learning-based hybrid joint angle estimation for flexible surgery robots, IEEE Robot. Autom. Lett. 5 (4) (2020) 6837–6844.
[112] O.M. Omisore, et al., Towards characterization and adaptive compensation of backlash in a novel robotic catheter system for cardiovascular interventions, IEEE Trans. Biomed. Circuits Syst. 12 (4) (2018) 824–838.
[113] J. Chen, H. Lau, Policy gradient-based inverse kinematics refinement for tendon-driven serpentine surgical manipulator, Int. J. Robot. Autom. 34 (3) (2019).
[114] M. Edgington, et al., Using joint probability densities for simultaneous learning of forward and inverse models, in: N.T. Siebel, J. Pauli (Eds.), IEEE IROS Int. Workshop on Evolutionary and Reinforcement Learning for Autonomous Robot Systems, Vol. 10, 2009, pp. 19–22.
[115] M. Giorelli, F. Renda, G. Ferri, C. Laschi, A feed-forward neural network learning the inverse kinetics of a soft cable-driven manipulator moving in three-dimensional space, in: 2013 IEEE/RSJ Int. Conf. on Intell. Robots and Systems, 2013, pp. 5033–5039, http://dx.doi.org/10.1109/IROS.2013.6697084.
[116] R.M. Grassmann, R.Z. Chen, N. Liang, J. Burgner-Kahrs, A dataset and benchmark for learning the kinematics of concentric tube continuum robots, in: 2022 IEEE/RSJ International Conference on Intelligent Robots and Systems, IROS, IEEE, 2022, pp. 9550–9557.
[117] D. Wu, et al., Data-driven modeling of complex hysteresis behaviour in MitraClip steerable catheters, in: Conference on New Technologies for Computer and Robot Assisted Surgery, Location: Paris, 2023.
[118] D. Wu, et al., Deep-learning-based compliant motion control of a pneumatically-driven robotic catheter, IEEE Robot. Autom. Lett. 7 (4) (2022) 8853–8860.
[119] S. Shakiba, et al., Modeling and compensation of asymmetric rate-dependent hysteresis of a miniature pneumatic artificial muscle-based catheter, Mech. Syst. Signal Process. 154 (2021) 107532, http://dx.doi.org/10.1016/j.ymssp.2020.107532.
[120] Z. Chen, X. Ren, M. Bernabei, V. Mainardi, G. Ciuti, C. Stefanini, A hybrid adaptive controller for soft robot interchangeability, IEEE Robotics Autom. Lett. 9 (1) (2023) 875–882.
[121] J.-S. Jang, ANFIS: adaptive-network-based fuzzy inference system, IEEE Trans. Syst. Man Cybern. 23 (3) (1993) 665–685.
[122] Y. Wang, et al., A CNNs-based of force and torque identification model for vascular interventional surgery robot, in: 2019 IEEE Int. Conf. on Mechatronics and Automation, ICMA, IEEE, 2019, pp. 2291–2296.
[123] G. Trovato, et al., Development of a colon endoscope robot that adjusts its locomotion through the use of reinforcement learning, Int. J. Comput. Assist. Radiol. Surg. 5 (4) (2010) 317–325.
[124] K. Iyengar, et al., Deep reinforcement learning for concentric tube robot control with a goal-based curriculum, in: 2021 IEEE Int. Conf. on Robot. and Automat., ICRA, IEEE, 2021, pp. 1459–1465.
[125] D. Wu, et al., Feasibility of using a long short-term memory network for robotic catheter control, in: 10 Th Conference on New Technologies for Computer and Robot Assisted Surgery, Date: 2020/09/28-2020/09/30, Location: Barcelona, Spain, 2020, pp. 68–69.
[126] D. Wu, Y. Zhang, M. Ourak, X.T. Ha, K. Niu, J. Dankelman, E. Vander Poorten, Deep-learning-based position control of a robotic catheter under environmental contact, in: 2022 International Symposium on Medical Robotics, ISMR, IEEE, 2022, pp. 1–7.
[127] M.A. Armin, et al., Learning camera pose from optical colonoscopy frames through deep convolutional neural network (CNN), in: Computer Assisted and Robotic Endoscopy and Clinical Image-Based Procedures, Springer, 2017, pp. 50–59.
[128] J.F. Lazo, C.-F. Lait, S. Moccia, B. Rosa, M. Catellani, M. de Mathelin, G. Ferrigno, P. Breedveld, J. Dankelman, E. De Momi, Autonomous intraluminal navigation of a soft robot using deep-learning-based visual servoing, in: 2022 IEEE/RSJ International Conference on Intelligent Robots and Systems, IROS, IEEE, 2022, pp. 6952–6959.
[129] B. Thamo, D. Hanley, K. Dhaliwal, M. Khadem, Data-driven steering of concentric tube robots in unknown environments via dynamic mode decomposition, IEEE Robot. Autom. Lett. (2022).
[130] X.T. HA, D. Wu, M. Ourak, G. Borghesan, A. Menciassi, E. Vander Poorten, Compliant motion control of robotic catheter based on long-short term memory network, in: 11th Conference on New Technologies for Computer/Robot Assisted Surgery Proceeding, 2022.
[131] J. Ritter, L. Karstensen, J. Langejürgen, J. Hatzl, F. Mathis-Ullrich, C. Uhl, Quality-dependent deep learning for safe autonomous guidewire navigation, Curr. Direct. Biomed. Eng. 8 (1) (2022) 21–24.
[132] L. Karstensen, J. Ritter, J. Hatzl, T. Pätz, J. Langejürgen, C. Uhl, F. Mathis-Ullrich, Learning-based autonomous vascular guidewire navigation without human demonstration in the venous system of a porcine liver, Int. J. Comput. Assist. Radiol. Surg. 17 (11) (2022) 2033–2040.
[133] H.-S. Song, B.-J. Yi, J.Y. Won, J. Woo, Learning-based catheter and guidewire-driven autonomous vascular intervention robotic system for reduced repulsive force, J. Comput. Des. Eng. 9 (5) (2022) 1549–1564.
[134] A. Segato, et al., Inverse reinforcement learning intra-operative path planning for steerable needle, IEEE Trans. Biomed. Eng. 69 (6) (2021) 1995–2005.
[135] D. Bruno, S. Calinon, G. Caldwell, Learning autonomous behaviours for the body of a flexible surgical robot, Auton. Robots 41 (2) (2017) 333–347.
[136] W. Xu, et al., Automate surgical tasks for a flexible serpentine manipulator via learning actuation space trajectory from demonstration, in: 2016 IEEE International Conference on Robotics and Automation, ICRA, IEEE, 2016, pp. 4406–4413.
[137] M.S. Malekzadeh, et al., Learning by imitation with the STIFF-FLOP surgical robot: a biomimetic approach inspired by octopus movements, Robot. Biomimetics 1 (1) (2014) 1–15.
[138] A.T. Tibebu, et al., Towards autonomous robotic catheter navigation using reinforcement learning, in: 4th Joint Workshop on New Technologies for Computer/Robot Assisted Surgery, 2014, pp. 163–166.
[139] L. Karstensen, et al., Autonomous guidewire navigation in a two dimensional vascular phantom, Curr. Direct. Biomed. Eng. 6 (1) (2020).
[140] S. Athiniotis, R. Srivatsan, H. Choset, Deep Q reinforcement learning for autonomous navigation of surgical snake robot in confined spaces, in: Proceedings of the the Hamlyn Symposium on Medical Robotics, London, UK, 2019, pp. 23–26.
[141] X. Tan, et al., Robust path planning for flexible needle insertion using Markov decision processes, Int. J. Comput. Assist. Radiol. Surg. 13 (9) (2018) 1439–1451.
[142] Y. Lee, et al., Simulation of robot-assisted flexible needle insertion using deep q-network, in: 2019 IEEE International Conference on Systems, Man and Cybernetics, SMC, IEEE, 2019, pp. 342–346.
[143] F. Meng, et al., Evaluation of a reinforcement learning algorithm for vascular intervention surgery, in: 2021 IEEE Int. Conf. on Mechatronics and Automation, ICMA, IEEE, 2021, pp. 1033–1037.
[144] J.-C. Latombe, Robot motion planning, Vol. 124, Springer Science & Business Media, 2012.

[145] A. Segato, et al., 3D neurosurgical simulator for training robotic steerable catheter agents using generative adversarial imitation learning, in: 2020 Int. Conf. on Robotics and Automation, FRA, 2020.
[146] Z. Li, et al., Robust path planning via learning from demonstrations for robotic catheters in deformable environments, 2024, arXiv preprint arXiv:2402.00537.
[147] D. Wu, Z. Li, M.H.D. Ansari, X.T. Ha, M. Ourak, J. Dankelman, A. Menciassi, E. De Momi, E. Vander Poorten, Comparative analysis of interactive modalities for intuitive endovascular interventions, IEEE Trans. Vis. Comput. Graphics (2024).
[148] X. Zhang, M.C. Palumbo, F. Perico, M. Magro, A. Fortuna, T. Magni, E. Votta, A. Segato, E. De Momi, Robotic actuation and control of a catheter for structural intervention cardiology, in: 2022 IEEE/RSJ International Conference on Intelligent Robots and Systems, IROS, IEEE, 2022, pp. 5907–5913.
[149] S. Çalışır, M.K. Pehlivanoğlu, Model-free reinforcement learning algorithms: A survey, in: 2019 27th Signal Processing and Communications Applications Conference, SIU, IEEE, 2019, pp. 1–4.
[150] A. Kienzlen, F. Jaensch, A. Verl, L. Cheng, Concept for a reinforcement learning approach to navigate catheters through blood vessels, in: 2022 28th International Conference on Mechatronics and Machine Vision in Practice, M2VIP, IEEE, 2022, pp. 1–4.
[151] M. Hessel, J. Modayil, H. Van Hasselt, T. Schaul, G. Ostrovski, W. Dabney, D. Horgan, B. Piot, M. Azar, D. Silver, Rainbow: Combining improvements in deep reinforcement learning, in: Proceedings of the AAAI Conference on Artificial Intelligence, Vol. 32, (1) 2018.
[152] A. Raffin, A. Hill, A. Gleave, A. Kanervisto, M. Ernestus, N. Dormann, Stable-baselines3: Reliable reinforcement learning implementations, J. Mach. Learn. Res. 22 (1) (2021) 12348–12355.
[153] F. Meng, S. Guo, W. Zhou, Z. Chen, Evaluation of an autonomous navigation method for vascular interventional surgery in virtual environment, in: 2022 IEEE International Conference on Mechatronics and Automation, ICMA, IEEE, 2022, pp. 1599–1604.
[154] Y. Cho, J.-H. Park, J. Choi, D.E. Chang, Sim-to-real transfer of image-based autonomous guidewire navigation trained by deep deterministic policy gradient with behavior cloning for fast learning, in: 2022 IEEE/RSJ International Conference on Intelligent Robots and Systems, IROS, IEEE, 2022, pp. 3468–3475.
[155] J. Kumar, C.S. Raut, N. Patel, Automated flexible needle trajectory planning for keyhole neurosurgery using reinforcement learning, in: 2022 IEEE/RSJ International Conference on Intelligent Robots and Systems, IROS, IEEE, 2022, pp. 4018–4023.
[156] W. Hu, H. Jiang, M. Wang, Flexible needle puncture path planning for liver tumors based on deep reinforcement learning, Phys. Med. Biol. 67 (19) (2022) 195008.
[157] J. Zhang, et al., Deformable models for surgical simulation: a survey, IEEE Rev. Biomed. Eng. 11 (2017) 143–164.
[158] W. Zhao, et al., Sim-to-real transfer in deep reinforcement learning for robotics: a survey, in: 2020 IEEE Symposium Series on Computational Intelligence, SSCI, IEEE, 2020, pp. 737–744.
[159] J. Tobin, et al., Domain randomization for transferring deep neural networks from simulation to the real world, in: 2017 IEEE/RSJ Int. Conf. on Intell. Robot. and Syst., IROS, IEEE, 2017, pp. 23–30.
[160] X.B. Peng, et al., Sim-to-real transfer of robotic control with dynamics randomization, in: 2018 IEEE International Conference on Robotics and Automation, ICRA, IEEE, 2018, pp. 3803–3810.
[161] S. Lin, et al., Lc-gan: Image-to-image translation based on generative adversarial network for endoscopic images, in: 2020 IEEE/RSJ Intt. Conf. on Intell. Robot. and Syst., IROS, IEEE, 2020, pp. 2914–2920.
[162] J. Sganga, et al., Offsetnet: Deep learning for localization in the lung using rendered images, in: 2019 International Conference on Robotics and Automation, ICRA, IEEE, 2019, pp. 5046–5052.
[163] T. Miller, Explanation in artificial intelligence: Insights from the social sciences, Artif. Intell. 267 (2019) 1–38.
[164] A.B. Arrieta, N. Díaz-Rodríguez, J. Del Ser, A. Bennetot, S. Tabik, A. Barbado, S. García, S. Gil-López, D. Molina, R. Benjamins, et al., Explainable artificial intelligence (XAI): Concepts, taxonomies, opportunities and challenges toward responsible AI, Inf. Fusion 58 (2020) 82–115.
[165] M.T. Ribeiro, S. Singh, C. Guestrin, Model-agnostic interpretability of machine learning, in: ICML Workshop on Human Interpretability in Machine Learning, 2016.
[166] L. Van der Maaten, G. Hinton, Visualizing data using t-SNE, J. Mach. Learn. Res. 9 (11) (2008).
[167] J.H. Friedman, Greedy function approximation: a gradient boosting machine, Ann. Stat. (2001) 1189–1232.
[168] A. Goldstein, A. Kapelner, J. Bleich, E. Pitkin, Peeking inside the black box: Visualizing statistical learning with plots of individual conditional expectation, J. Comput. Graph. Stat. 24 (1) (2015) 44–65.
[169] M.D. Zeiler, R. Fergus, Visualizing and understanding convolutional networks, in: Computer Vision–ECCV 2014: 13th European Conference, Zurich, Switzerland, September 6-12, 2014, Proceedings, Part I, Vol. 13, Springer, 2014, pp. 818–833.
[170] E. Parliament, C. of the European Union, Artificial intelligence act: Regulation laying down harmonised rules on artificial intelligence and amending certain union legislative acts, in: Proposal for Regulation COM/2021/206 Final, Brussels, Belgium, 2021.
[171] B. Fei, et al., The safety issues of medical robotics, Reliab. Eng. Syst. Saf. 73 (2) (2001) 183–192.
[172] C. Liu, et al., Algorithms for verifying deep neural networks, Found. Trends Optim. 4 (3–4) (2021) 244–404.
[173] R.H. Wortham, et al., Improving robot transparency: Real-time visualisation of robot AI substantially improves understanding in naive observers, in: 2017 26th IEEE Int. Symposium on Robot and Human Interactive Communication, RO-MAN, IEEE, 2017, pp. 1424–1431.
[174] A. Pore, et al., Safe reinforcement learning using formal verification for tissue retraction in autonomous robotic-assisted surgery, in: 2021 IEEE/RSJ Int. Conf. on Intell. Robot. and Syst., IEEE, 2021, pp. 4025–4031.
[175] J. Garcıa, et al., A comprehensive survey on safe reinforcement learning, J. Mach. Learn. Res. 16 (1) (2015) 1437–1480.
[176] A.K. Manrai, et al., Genetic misdiagnoses and the potential for health disparities, N. Engl. J. Med. 375 (7) (2016) 655–665.
[177] A.R. Benaim, et al., Analyzing medical research results based on synthetic data and their relation to real data results: systematic comparison from five observational studies, JMIR Med. Inf. 8 (2) (2020) e16492.
[178] R.J. Chen, et al., Synthetic data in machine learning for medicine and healthcare, Nat. Biomed. Eng. (2021) 1–5.
[179] S. Tonekaboni, et al., What clinicians want: contextualizing explainable machine learning for clinical end use, in: Machine Learning for Healthcare Conference, PMLR, 2019, pp. 359–380.